ANNUAL REVIEWS

Annual Review of Fluid Mechanics

The Fluid Mechanics of Ocean Microplastics

Michelle H. DiBenedetto

Department of Mechanical and Aerospace Engineering, Princeton University, Princeton, New Jersey, USA; email: mdiben@princeton.edu

Annu. Rev. Fluid Mech. 2026. 58:355–82

First published as a Review in Advance on October 2, 2025

The *Annual Review of Fluid Mechanics* is online at fluid.annualreviews.org

https://doi.org/10.1146/annurev-fluid-120423-012604

Keywords

microplastics, plastic pollution, ocean transport, surface waves

Abstract

Microplastic pollution is now ubiquitous in marine environments, posing risks to ecosystem and human health. In order to assess and mitigate this threat, we require accurate prediction of microplastic fate and transport in the ocean. While progress has been made studying global-scale transport pathways, our models often fall short at smaller scales; processes such as vertical transport, horizontal dispersion, particle transformation, and boundary fluxes (e.g., at beaches and the air–sea interface) remain poorly understood. The difficulty lies in the physical features of plastic particles: namely, near-neutral buoyancy in seawater, finite size, and irregular shape. These complexities are compounded by the multiscale forcing from waves and turbulence near the ocean surface where microplastics tend to reside. This review synthesizes recent advances in the fluid dynamics of marine plastic transport, emphasizing the role of fluid–particle interactions in ocean flows and highlighting outstanding challenges.

1. INTRODUCTION

Microplastic: plastic particle commonly defined in the size range of 1 μm to 5 mm

Garbage patch: relatively high concentration of floating plastic that exists in areas of surface convergence associated with the subtropical gyres

Plastic fate and transport predictions are a crucial component of marine pollution mitigation and cleanup efforts, and those predictions require a fundamental understanding of how microplastics interact with their environment. At global scales, progress has been made by leveraging ocean circulation models and surface observations, bringing attention to the well-documented garbage patches, or subtropical gyres where floating plastic tends to accumulate. In contrast, much less is understood about the smaller-scale processes that affect plastics away from the ocean surface: Vertical transport, fragmentation, and coastal deposition all remain poorly understood, but they are key to closing the ocean plastic budget. Investigating these pathways is a daunting task, given that plastic particle sizes range from the macro- to nanoscale, and because fluid forcing varies from large-scale currents to small-scale turbulence. Beyond the intricate links to fluid mechanics, the multidisciplinary aspects of microplastics in the ocean pose additional challenges, with intersections across chemical and biological oceanography.

1.1. Plastic Pollution Background

Celebrated for their utility and low cost, plastics have enabled many aspects of modern life. However, the very properties that make plastic so useful, e.g., extreme durability and chemical inertness, also inhibit plastic's degradation and remineralization (Chamas et al. 2020). As a consequence, it is possible that nearly all plastic ever produced, beyond the material that has been incinerated, still exists on Earth (Thompson et al. 2024). Once it enters the environment, plastic tends to fragment into smaller pieces, facilitating widespread dispersal. These characteristics make plastic a persistent pollutant that may be impossible to completely remediate (Worm et al. 2017, MacLeod et al. 2021). Thus, plastic pollution has become the new normal.

In the ocean, plastic pollution was initially reported in 1972 when small plastic pellets were collected in biological surveys (Carpenter & Smith 1972). By 1997, observations began showing high levels of plastic accumulating in the Pacific (Moore et al. 2001). The term microplastics was not generally used until 2004 (Thompson et al. 2004). Since then, there has been an explosion of research activity on the topic, driven partly by the scale and visibility of the problem. Images of floating plastic litter in surface waters, on coastlines, and in the stomachs of marine animals have galvanized public concern and motivated over 4,500 research articles (Landrigan et al. 2023). At the same time, significant quantities of plastic reside in areas where it is harder to track and quantify; for example, plastic has been found in the deep sea (Woodall et al. 2014) and within sea ice (Obbard et al. 2014).

The impacts of plastic pollution on living organisms can generally be categorized as either physical or chemical. Physically, entanglement and ingestion by marine animals can lead to injury, malnutrition, and death. Chemically, plastic can act as a vector that transports and releases toxic additives or adsorbed pollutants into the organisms that ingest it (Worm et al. 2017). Human health is also at risk: Research suggests that exposure to plastic, either through environmental contact or product use, can cause a variety of detrimental effects (Landrigan et al. 2023). Beyond the damage this pollution inflicts to ecosystems and human health, plastic also intersects with climate change by affecting the ocean's biological pump (Wieczorek et al. 2019, Guerrini et al. 2023) and altering carbon cycling in the environment (MacLeod et al. 2021).

1.2. Ocean Plastic Budget

Since the 1950s, global plastic production has been increasing annually and is expected to continue rising, with over 360 million metric tons (Mt) of plastic waste generated in 2020 alone (OECD 2024). Although approximately half of plastic waste is landfilled (with smaller fractions

incinerated or recycled), a significant portion remains mismanaged, allowing it to enter the environment (Geyer et al. 2017, OECD 2024). In 2016, an estimated 9–23 Mt of mismanaged plastic entered aquatic ecosystems, including rivers, oceans, and lakes (Borrelle et al. 2020, Lau et al. 2020). Projections under a business-as-usual scenario predict that this figure could reach 35.8–90.0 Mt per year by 2030 (Borrelle et al. 2020).

Once plastic pollutes the ocean, it becomes harder to track. More than half of all plastic produced is composed of material that is less dense than seawater, so we expect it to float at the ocean surface (Geyer et al. 2017). However, observational studies indicate that only 0.08–0.58 Mt of plastic is currently floating at the ocean surface (van Sebille et al. 2015, Isobe et al. 2021), multiple orders of magnitude less than the amount estimated to enter the oceans each year (Jambeck et al. 2015, Borrelle et al. 2020). The discrepancy between these values is often termed the missing plastic (Law 2017).

Various sources of uncertainty in the plastic pollution mass balance may contribute to the missing plastic problem: (*a*) Not all of the plastic in the ocean is floating at the ocean surface. Plastic accumulates in other marine reservoirs that are harder to quantify, including coastlines, the water column, the seafloor, sediments, sea ice, and marine life. (*b*) Surface values could be underestimated, e.g., plastic debris continuously fragments in the environment and smaller plastic particles are more challenging to measure. (*c*) Emission estimates may be too high; e.g., Weiss et al. (2021) argue that emissions to the ocean from rivers have been vastly overestimated, which may account for a portion of the discrepancy.

1.3. Challenges in Studying the Fluid Dynamics of Plastic Transport in the Ocean

The literature on microplastics is rapidly expanding, owing to heightened public attention and the interdisciplinary nature of the topic, which touches on a variety of fields including material science, chemistry, environmental policy, and oceanography. Numerous reviews address this topic, including transport focused on physical oceanography (van Sebille et al. 2020), ocean mixed layer transport studied via large eddy simulations (Chamecki et al. 2019), and a fluid dynamics perspective (Sutherland et al. 2023b), among others (Law 2017, Poulain-Zarcos et al. 2024). Readers are referred to these sources for more information.

This review, in contrast, focuses on the smaller-scale processes that affect how microplastics are transported by ocean flows. This is a nontrivial topic for two primary reasons: (*a*) The physical properties (size, shape, and density) of microplastics differ from traditionally studied environmental particles like sediment or bubbles, and (*b*) interactions among waves, turbulence, and particles in the ocean are not well-understood, especially for finite-size, near-neutrally buoyant, and nonspherical particles such as microplastics.

With those challenges in mind, I aim to review the recent work studying the fluid mechanics of microplastics, helping to illustrate how microplastics research has uncovered underexplored facets of oceanic flows and identified new regimes for particle–flow interactions. I also detail relevant background for those interested in working on this topic and highlight specific fluid dynamics problems and outstanding questions, including how microplastics cross between different oceanic compartments, e.g., surface waters, the air–sea interface, and beaches. I also emphasize that fluid dynamics is only one piece of the puzzle—ultimately, unraveling the complex behaviors of microplastic fate and transport requires interdisciplinary research.

I begin by describing microplastics and their relevant characteristics in more detail. I then turn our focus to the unique fluid dynamics questions in this field, namely, transport at the ocean surface and at boundaries. Though much of this work mirrors research on particles in turbulence, one

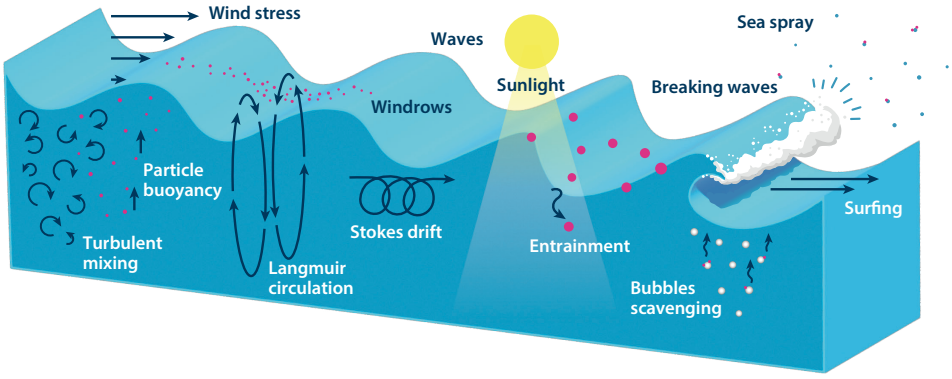

Figure 1

Schematic depicting some of the most relevant processes to the fate and transport of microplastics at the ocean surface.

major difference is the consideration of ocean waves, which affect both the vertical and horizontal transport of microplastics, as depicted in **Figure 1**. I finish by summarizing outstanding questions and highlighting important future areas of research.

2. MICROPLASTICS

2.1. Properties

This section begins by defining microplastics and reviewing their common properties in the environment relevant to their fluid mechanics.

2.1.1. Definitions. Microplastics are often defined as plastic particles between 1 μm and 5 mm in size (Cózar et al. 2014, Eriksen et al. 2014), though there are varying definitions in the literature (Hartmann et al. 2019). Larger particles are often termed mesoplastic (5–20 mm) and macroplastic (>20 mm) (Napper & Thompson 2023). Nanoplastics (<1 μm) have also generated recent interest, but methods to detect and analyze them in the environment are still being developed and thus there are fewer studies on the topic (Moon et al. 2024). While macroplastics make up the majority of the plastic mass in the ocean, microplastics are thought to be the more abundant size class by number (Kaandorp et al. 2023). Microplastics originate both from direct entry into the ocean and from the fragmentation of larger plastic debris (Andrady 2017). Their variable origin implies a variety of shapes, including microfibers, flat planar fragments, and spherical pellets such as nurdles, as shown in **Figure 2**.

Microfiber: common microplastic pollutant generated from textiles; can also refer to nonplastic fibers including cotton

Fragment: planar piece of plastic fragmented from larger plastic

Nurdle: preproduction plastic pellet that is slightly oblong in shape, often 3–5 mm in size

2.1.2. Material properties. The most common polymers found at the ocean surface are polypropylene and low- and high-density polyethylene (Bond et al. 2018), with density ρ_p ranging from 0.9 to 0.97 g/cm^3 (Andrady 2017). Denser polymers include polystyrene, PET, nylon, and PVC, with densities ranging from 1.04 to 1.4 g/cm^3 (Andrady 2017). Therefore, microplastics are near-neutrally buoyant in seawater (with fluid density $\rho_f \approx 1.025$ g/cm^3); indeed, one study presented a model for the distribution of all microplastics densities and found a modal value of $\rho_p \approx 1$ g/cm^3 (Kooi & Koelmans 2019). Plastic density is not necessarily constant and can change over time due to biological growth (Kooi et al. 2017) and weathering (Andrady & Koongolla 2022). The density of plastics will also not necessarily be uniform, which can affect their dynamics (e.g., see Angle et al. 2024). Finally, while most plastics are hydrophobic when produced, weathering and photodegradation can make them more hydrophilic (Andrady & Koongolla 2022).

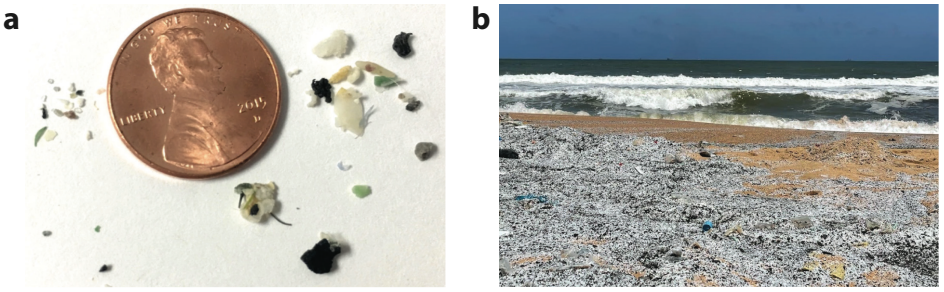

Figure 2

Microplastic examples. (*a*) Microplastics collected from the surface of San Francisco Bay with a US penny (diameter 19.05 mm) for reference. (*b*) Aftermath of the *M/V X-Press Pearl* nurdle spill in May 2021 on a beach in Sri Lanka. Panel adapted from de Vos et al. (2021) (CC BY 4.0).

2.1.3. Particle size distribution. Particle size distributions are key to modeling particle transport, but disagreements remain regarding the form, stationarity, and universality of microplastic size distributions (Kooi & Koelmans 2019). Power-law size distributions have been proposed based on fits to observations of larger microplastics; these observations tend to show a peak near 1 mm, as shown in **Figure 3*a*** (Kaandorp et al. 2021). However, these distributions may be impacted by measurement errors (e.g., size-selection sampling bias, reduced sensitivity to smaller particles) or sorting of microplastics in the environment. Based on fragmentation models, these modeled distributions assume that the smaller microplastics are being produced from the larger ones within a closed system. In reality, fragmentation likely occurs over longer timescales than the transport processes that sort particles by size (Kaandorp et al. 2021). Some organisms may also show size selectivity in their microplastic ingestion, which could affect particle size distribution measurements (Scherer et al. 2017).

2.1.4. Relevant nondimensional parameters. This section summarizes some common nondimensional parameters and the regimes microplastics typically occupy.

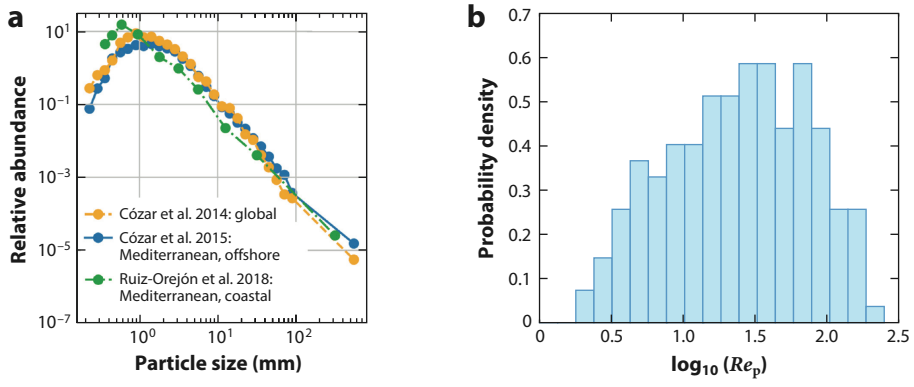

Figure 3

Microplastic characteristics. (*a*) Observations of microplastic particle size distributions. Panel adapted from Kaandorp et al. (2021) (CC BY 4.0). (*b*) Particle Reynolds numbers of microplastic observations using rise velocity and longest length scale. Data from DiBenedetto et al. (2023).

Langmuir circulation: counterrotating vortices aligned with the wind that create strong surface convergence zones, downwelling jets, and long visible windrows where debris and/or foam can accumulate

Maxey–Riley–Gatignol equation: describes the forces on an inertial, spherical particle in an unsteady fluid flow

2.1.4.1. Volume fraction. Microplastic concentrations in the open ocean are often ≤1 particle/m^3. Therefore, they typically fall into a dilute regime with low volume fractions, and assuming a one-way coupling between the particles and fluid is appropriate (i.e., the particles do not affect the fluid). This may break down near flow features that preferentially concentrate particles (e.g., fronts and Langmuir circulation) or near isolated sources of plastic pollution (e.g., **Figure 2*b*** shows the aftermath of the largest nurdle spill to date).

2.1.4.2. Particle Reynolds number. Using the microplastic terminal rise/settling velocity in quiescent water w_t, we define the particle Reynolds number $Re_p = d_p w_t/\nu$, where d_p is the diameter (or characteristic length) of the (potentially nonspherical) particle and ν is the fluid kinematic viscosity. The smallest microplastics have $Re_p \ll 1$ and exist in the Stokes flow regime. However, many of the microplastics measured at the ocean surface fall within an intermediate particle Reynolds number regime. **Figure 3*b*** shows data from net tows in the Pacific where $Re_p \approx 2$–300 for particle sizes ranging from 0.5 to 30 mm (defined by particle maximum length). At these intermediate Reynolds numbers, neither viscosity nor inertia can be neglected, and empirical parameterizations are often needed to describe the drag on a particle [e.g., the Schiller–Naumann equation (Clift et al. 2005)]. Some parameterizations can account for idealized nonspherical particles (e.g., Fröhlich et al. 2020), but irregular shape and unsteadiness continue to pose a challenge. For example, tumbling and fluttering are common for particles at intermediate to high Reynolds numbers, further complicating their dynamics (e.g., Will et al. 2021, Tinklenberg et al. 2023).

2.1.4.3. Stokes number. The Stokes number describes the relative importance of a particle's inertia to its motion in a fluid flow. To derive an expression for it, we consider the equation of motion for a spherical point particle, often referred to as the Maxey–Riley–Gatignol equation (Gatignol 1983, Maxey & Riley 1983). For simplicity, we neglect the Faxén corrections and the Basset history force, including only forces due to gravity, buoyancy, fluid acceleration, added mass, and drag, giving the following expression:

$$m_p \frac{\mathrm{d}\mathbf{u}_p}{\mathrm{d}t} = (m_p - m_f)\mathbf{g} + m_f \frac{\mathrm{D}\mathbf{u}_f}{\mathrm{D}t} - C_m m_f \left(\frac{\mathrm{d}\mathbf{u}_p}{\mathrm{d}t} - \frac{\mathrm{D}\mathbf{u}_f}{\mathrm{D}t} \right) - \frac{1}{2} C_D \rho_f A |\mathbf{u}_p - \mathbf{u}_f| (\mathbf{u}_p - \mathbf{u}_f). \quad 1.$$

Here, m_p is the mass of the particle, m_f is the mass of the fluid displaced by the particle, C_m is the added mass coefficient ($C_m = 1/2$ for a submerged sphere), C_D is the drag coefficient, and A is the particle's frontal area. The particle velocity $\mathbf{u}_p$ and the undisturbed fluid velocity $\mathbf{u}_f$ are both defined at the particle's centroid. The derivatives $\mathrm{d}/\mathrm{d}t$ and $\mathrm{D}/\mathrm{D}t$ correspond to particle-following and fluid-following time derivatives, respectively, and $\mathbf{g} = -g\hat{e}_z$ is the gravitational acceleration vector. In Stokes flow ($Re_p \ll 1$), we find $C_D = 24/Re_p$, whereas for intermediate Re_p, we can use the Schiller–Naumann approximation $C_D \approx 24/Re_p(1 + 0.15Re_p^{0.687})$, which applies up to $Re_p \approx 800$ (Clift et al. 2005). In this case, Re_p is defined with the absolute slip velocity $Re_p = |\mathbf{u}_p - \mathbf{u}_f| d_p/\nu$. Next, we rearrange and rewrite Equation 1 as

$$\frac{\mathrm{d}\mathbf{u}_p}{\mathrm{d}t} = (1 - \beta)\mathbf{g} + \beta \frac{\mathrm{D}\mathbf{u}_f}{\mathrm{D}t} - \frac{\mathbf{u}_p - \mathbf{u}_f}{\tau_p}, \quad 2.$$

where $\beta = (1 + C_m)/(\rho_p/\rho_f + C_m)$ and τ_p is the particle relaxation timescale. This timescale characterizes how long it takes a particle to respond to changes in the flow. For a spherical point particle, including effects from both drag and added mass, the relaxation time can be written as

$$\tau_p = \frac{4}{3\nu} \frac{d_p^2 \left(\frac{\rho_p}{\rho_f} + C_m \right)}{C_D Re_p}. \quad 3.$$

Alternative definitions exist (e.g., see Brandt & Coletti 2022). Note that the terminal rise/settling velocity can be related to τ_p here by $w_t = -\tau_p(1 - \beta)g$. While this equation applies to spherical

Table 1 Example values for buoyant spherical microplastics in ocean turbulence

Diameter d_p (mm)	Specific gravity ρ_p/ρ_f	w_t (cm/s)	Re_p	St (low)	St (high)	d_p/η (low)	d_p/η (high)
0.05	0.9	0.014	0.007	2×10^{-4}	2×10^{-2}	0.05	0.5
0.1	0.9	0.055	0.05	8×10^{-4}	8×10^{-2}	0.1	1
1	0.97	0.96	9.6	5×10^{-2}	5×10^{0}	1	10
1	0.9	2.4	24	3×10^{-2}	3×10^{0}	1	10
5	0.97	5.2	260	3×10^{-1}	3×10^{1}	5	50
5	0.9	11	550	2×10^{-1}	2×10^{1}	5	50

We use Stokes drag for particles with $Re_p < 1$ here and the Schiller–Naumann approximation for $Re_p > 1$. We use Equation 3 to estimate τ_p using $Re_p = w_t d_p/\nu$. Low and high values correspond to $\varepsilon = 10^{-6}$ and 10^{-2} m^2/s^3, respectively.

point particles, defining τ_p can become increasingly intractable as particles become nonspherical, become large relative to the scales of the flow, or become neutrally buoyant without a clearly defined slip velocity.

Finally, we can define the Stokes number $St = \tau_p/\tau_f$, where τ_f is a relevant fluid timescale; it is often defined by the Kolmogorov timescale in turbulence or the wave period in waves. To estimate τ_f in the ocean, we will use the Kolmogorov timescale $\tau_\eta = \sqrt{\nu/\varepsilon}$ based on the turbulent energy dissipation rate ε, which varies widely in the ocean. In the ocean mixed layer, average values approach $\varepsilon \approx 10^{-6}$–$10^{-5}$ m^2/s^3 (Fuchs & Gerbi 2016), but measurements under breaking waves in the ocean surface and surf zone have shown $\varepsilon \approx 10^{-4}$–$10^{-2}$ m^2/s^3 (Sutherland & Melville 2015, Thomson et al. 2016, Zippel et al. 2020). We report typical St values for the low and high ends of these ranges for a variety of microplastic sizes in **Table 1**. Note that turbulence dissipation is often much lower than these values in the ocean, especially below the mixed layer. In many cases, we expect $St \ll 1$ where inertial effects can be neglected and the microplastics resemble fluid tracers with a prescribed rise/settling velocity (also summarized by Chamecki et al. 2019). However, even small relative inertia (e.g., $St \approx 10^{-2}$) can result in accumulated deviations from the fluid velocity over time, resulting in appreciable differences in overall transport between the particles and fluid tracers (Ouellette et al. 2008).

2.1.4.4. Relative size. Because plastic debris covers a wide size range, microplastics can be larger than the smallest fluid length scales, i.e., $d_p/\eta > 1$, where $\eta = (\nu^3/\varepsilon)^{1/4}$ is the Kolmogorov length scale (**Table 1**). For reference, η is approximately 1 mm and 0.1 mm for ε values of 10^{-6} and 10^{-2} m^2/s^3, respectively. In the regime where $d_p/\eta \gg 1$, larger particles will filter out smaller scale motions and can no longer be treated as point particles. Finite size can also change the relative importance of forces on particles, particularly increasing the contributions of added mass and Basset history (see Section 4.3.1).

2.2. Transformation

In the ocean, microplastics can transform over time. The two most relevant processes controlling this transformation are fragmentation and aggregation.

2.2.1. Fragmentation. Over time, plastic in the environment fragments into smaller pieces. This fragmentation primarily occurs due to mechanical abrasion, ultraviolet (UV) radiation, and biological activity. UV radiation causes plastic to become more brittle, which can help accelerate fragmentation over time. The chemistry of plastic degradation processes is reviewed in detail by Andrady & Koongolla (2022). These processes occur over long timescales [some estimates place

marine degradation rates around 1–100 μm/year (Chamas et al. 2020)], so they are difficult to observe with controlled experiments.

Laboratory studies have begun to examine the role of turbulence in fragmentation. In theory, flow-induced strain can deform and break particles down to sizes on the order of the Kolmogorov length. Using flexible glass fibers as model plastics, experiments by Brouzet et al. (2021) showed that turbulence could deform the fibers and fragment them down to the size of the elastic length, which demarcates the transition between rigid motion and deformations by the turbulence (Brouzet et al. 2014). They estimated that in turbulent breaking waves, the elastic length may be as small as 2 mm. Experiments and analysis of deformable discs in turbulence expanded on the fiber studies, although only deformation was observed without fragmentation (Verhille 2022).

Overall, experimental results emphasize that while ocean turbulence may be able to break macrodebris into millimeter-sized particles, it is not typically strong enough to fragment them further. One exception may be near coastlines, where mechanical abrasion of plastic by sand and other material can accelerate fragmentation, especially when waves break directly onto sand or rocks (Chubarenko et al. 2020). Therefore, degradation rates are expected to vary spatially, with coastal regions having potentially higher degradation rates than the open ocean.

2.2.2. Aggregation. Particle aggregation has been widely studied in the context of marine biogeochemistry. For example, particle collision and settling models have been developed to describe marine snow and other aggregates (reviewed in Burd & Jackson 2009). Microplastics can also aggregate with particles in the ocean, and existing aggregation models may need to be adapted to account for the synthetic nature and distinct properties of microplastics. Some research has begun examining microplastic-specific aggregation processes. For example, when microplastics encounter bacteria that form a biofilm, they can become biofouled (Michels et al. 2018). Microplastics can also aggregate with sediment (Sutherland et al. 2023a) or become incorporated into marine and freshwater snow (Porter et al. 2018, Parrella et al. 2024). The size, density, and heterogeneous composition of microplastics will alter the transport properties of the bulk aggregate, affecting everything from settling velocities to chemical interactions. Because these phenomena vary with ocean chemistry, biology, and fluid mechanics, predicting the fate and transport of microplastic/natural particle aggregates remains a challenging and evolving area of research.

Though aggregate properties vary widely, their growth and breakup can always be mediated by the flow. For example, weak turbulence can promote growth by enhancing encounter rates between particles, whereas strong turbulence can cause breakup via shear (Rahmani et al. 2022, Song & Rau 2022). It follows that the Kolmogorov length is an upper bound on the size of aggregates. Fronts and other forms of surface convergence can accumulate plastic and other material in the ocean, enhancing aggregation likelihood (D'Asaro et al. 2018, Wang et al. 2022). In more quiescent waters (e.g., below the mixed layer), aggregate formation is enhanced by differential settling of particles (Lick et al. 1993). While typically studied in the context of multiple settling particles, here it may be relevant to consider the interaction between a rising microplastic and settling organic particle. This large differential in settling/rising could potentially further increase encounter rates.

2.3. Measurement Techniques

Making high-quality, highly resolved measurements of microplastics in space and time remains a challenge in the ocean. Some of the common techniques are reviewed here.

2.3.1. Direct measurements. Directly sampling for microplastics is labor intensive. Most ocean measurements have been made with towed surface nets (e.g., Neuston nets) originally designed for plankton sampling. Other direct methods use pumps or grab samples, both of which are filtered to isolate particulates. After filtering, particles must be separated from any organic material and confirmed to be plastic, either through chemical identification (usually Fourier-transform infrared or Raman spectroscopy) or visual inspection, which can be biased (Stark 2022). Laboratory settings are frequently contaminated by microplastics, so reference blank samples are needed when processing ocean-sourced plastic.

Neuston net: a net that skims the ocean surface layer, typically sampling to a depth of 10–20 cm

The concentration of microplastics in a given sample can be influenced by the sampling device. Nets typically have 200–330-μm mesh to avoid clogging with organic material, and they are often towed to sample a volume of approximately 10,000 L, whereas bottle grab samples can have a volume of 1–10 L and will be able to capture particles smaller than the net mesh size (Watkins et al. 2021). One meta-analysis of microplastic observation studies found that the average concentration of particles was negatively correlated with the volume of water measured (Watkins et al. 2021). This can be explained by the presence of local hot spots in microplastic concentration (Cohen et al. 2019), which complicate the picture of a uniform dilute suspension. While peak net-tow microplastic surface concentrations typically vary from $\mathcal{O}(10^0)$ to $\mathcal{O}(10^1)$ particles/m^3, or $\leq$1 particles/m^2 of ocean surface (Law et al. 2010, Law 2017, Poulain et al. 2019), grab samples have reported concentrations up to $\mathcal{O}(10^2)$–$\mathcal{O}(10^3)$ particles/L (Barrows et al. 2017, Watkins et al. 2021). These high concentrations may be related to preferential concentration by fluid flows (see Section 3.2.1). The flow can affect measurements in other ways: Vertical mixing can reduce surface concentration relative to quiescent conditions (Kukulka et al. 2012), and waves may also bias measurements if crests and troughs are not sampled uniformly (DiBenedetto 2020). In summary, while there have been many reported observations of microplastics, sampling methods are inconsistent, the measurements are spatiotemporally sparse, and measurements are predominantly from the ocean surface, making it challenging to quantify microplastic pollution at global scales from observations alone.

2.3.2. Indirect measurements. Because microplastics in the ocean are relatively undersampled, developing robust indirect sampling methods has been of interest. For example, Colson & Michel (2021) developed a flow-through system that identifies plastic particles via spectral impedance. Remote sensing methods have also been proposed, though measuring microplastics from satellite or airborne imagery is challenging due to their small size and dilute concentration. One proof-of-concept study described how satellites could be optimized to detect ocean surface plastic, focusing on detecting areas of high plastic concentration in filamentous structures, hypothesizing that fronts and windrows may have locally high plastic concentration (Cózar et al. 2024). Such an approach may be feasible if future satellite sensors have dedicated spectral bands to isolate plastic from other material.

Another study, hypothesizing that surfactants associated with microplastics may dampen wave energy, inferred microplastic concentration based on a mismatch between satellite observations of ocean surface roughness and roughness estimates based on modeled wind speeds (Evans & Ruf 2022). However, while surfactants can dampen waves, there are many naturally occurring surfactants in the ocean, so it is not clear that this effect can be reliably attributed to the presence of plastic. Moreover, the observed surface roughness anomalies could be caused by other physical phenomena that correlate with the placement of the subtropical gyres where plastic accumulates, e.g., wave–current interactions (Rapizo et al. 2018). Laboratory experiments also examined whether the mere presence of plastic could dampen waves; however, they found that plastic concentrations in the ocean are too low for the effect to be detectable (Sun et al. 2023, Calvert et al. 2025).

3. HORIZONTAL TRANSPORT AT THE OCEAN SURFACE

3.1. Wave-Induced Horizontal Transport

Stokes drift: horizontal transport generated by surface gravity waves that arises from a Lagrangian average of the wave-induced velocity field

Surface gravity waves are a defining feature of the ocean surface and nearshore and must be considered when studying the transport of buoyant objects that accumulate near the surface. Past research in this area has focused on buoys, sea ice, sargassum, oil droplets, and other debris. However, the properties of plastic debris are fundamentally different from these other floating objects, motivating the development of a distinct research area.

We can describe irrotational wave motion using linear wave theory, which applies to waves with small wave steepness $\epsilon = ka \ll 1$, where a is the wave amplitude and k is the wavenumber. Linear wave theory breaks down as waves become too steep or when waves become too shallow (the wave height approaches the water depth h). In deep water ($kh \gg 1$), the wave-induced velocity field described by linear wave theory is

$$u = \epsilon c \exp kz \cos(kx - \omega t), \quad 4.$$

$$w = \epsilon c \exp kz \sin(kx - \omega t). \quad 5.$$

Here, ω is the wave frequency and is related to the wavenumber via the deep-water dispersion relationship $\omega = \sqrt{gk}$, where g is acceleration due to gravity, $c = \omega/k$ is the phase speed, and u and w are the respective horizontal and vertical velocities in the x and z direction. The mean free surface is defined at $z = 0$, with $z < 0$ downward.

As a wave passes, fluid elements trace orbits with induced velocities $\mathcal{O}(\epsilon)$ and no mean Eulerian flow. However, from a Lagrangian viewpoint, waves induce an $\mathcal{O}(\epsilon^2)$ mean transport in their direction of propagation known as Stokes drift (van den Bremer & Breivik 2018). In deep water, the Stokes drift can be described by

$$u_{SD} = \epsilon^2 c \exp 2kz. \quad 6.$$

The sum of the Stokes drift and the mean Eulerian velocity is the mean Lagrangian velocity. One way to physically explain Stokes drift is that the Lagrangian fluid particles oversample the wave crest (where $u > 0$) and undersample the wave trough (where $u < 0$) relative to an Eulerian observer. Another contribution to Stokes drift arises from the fact that wave orbital velocities decay with depth in deep water; therefore, as a fluid particle travels in a wave orbital, it has faster forward velocity at the top of its orbital relative to its backward velocity at the bottom of the orbital.

3.1.1. Drifting in nonbreaking waves. The transport of finite-sized particles can differ from fluid particles in nonbreaking waves. One study used the Maxey–Riley–Gatignol equation to study particle transport in linear waves (DiBenedetto et al. 2022); they found that heavy (light) particles had reduced (enhanced) horizontal drift relative to the Stokes drift. The particle's relative inertia altered the particle's wave orbital size, such that heavy particles traced a smaller orbit whereas light particles traced a larger one. This effect is largest for high Stokes numbers and for particles that are farther from neutral buoyancy. A study that considered bubble transport under breaking waves predicted this effect could increase transport by up to 10% (Ruth et al. 2022). However, this model only applies to submerged particles, as it does not consider any free surface effects.

Buoyant finite-sized particles can float and bob at the free surface. First we consider particles much smaller than the wavelength λ, i.e., $d_p/\lambda \ll 1$, such that effects of the particle on the waves are small, yet the particle is large enough that surface tension can be neglected; this is given by the limit $d_p > \lambda_c$, where the capillary length in water is $\lambda_c \approx 2.7$ mm (given $\lambda_c = \sqrt{\gamma/\rho g}$ and the fluid surface tension γ). Surface tension effects cannot be neglected for particles smaller than this and

are discussed later. Research on floating particles is often motivated by both microplastic transport and the transport of larger plastic debris.

Like a submerged particle, a floating object will experience buoyancy, gravity, drag, and inertial forces, but it will also feel what is sometimes called a slope-sliding force due to the free surface slope and associated horizontal hydrostatic pressure gradient (Rumer et al. 1979). Huang et al. (2016) found that including this force in a transport model resulted in an increase in net drift of floating objects consistent with observations by Huang et al. (2011). Calvert et al. (2021) found similar results where dynamic buoyancy due to variable submergence causes a net drift enhancement for a spherical object when averaged over a wave period (up to 50% enhancement for $d_p/\lambda \lesssim 0.05$). Experiments showed that as the object size increases, so too does the drift enhancement; object shape was also considered in these experiments, showing enhanced drift of discs and spheres (Calvert et al. 2024).

As the object size increases relative to the wavelength, the floating object will begin interacting with the waves through diffraction and radiation, further affecting its drift. One study predicted a factor of two increase over the Stokes drift for objects with $d_p/\lambda \approx 0.1$ (Xiao et al. 2024). The authors derived a "diffraction-modified Stokes drift" using potential flow theory and the boundary element method (BEM) to solve for diffraction and radiation. Numerical simulations validated their result and showed that this effect can be attributed to a diffracted standing wave pattern that develops in the reference frame of the object. While this drift enhancement has also been observed in the lab (Xiao et al. 2025), the theory tended to underpredict the enhancement with increased object size ($d_p/\lambda > 0.1$, as shown in **Figure 4*e***). These studies suggest that nonlinear effects not captured by the linear BEM theory become increasingly important as object size increases, and that even for small objects, the transport implications of wave diffraction and radiation are nonnegligible.

3.1.2. Horizontal transport in breaking waves. When waves break, the surface transport is increased relative to the Stokes drift through a surfing effect (Deike et al. 2017, Pizzo et al. 2019), depicted in **Figure 4*a***. Surfing particle transport can approach the wave phase speed c, which is always faster than the Stokes drift velocity. This enhanced drift is concentrated near the surface where the waves break, but it has also been observed for bubbles below the surface, as shown in **Figure 4*d***. Beyond increased horizontal transport, breaking waves also generate turbulence that can mix microplastics down below the surface. Therefore, we expect only floating objects that are buoyant enough to remain at the surface during a breaking event will be able to surf the waves. Macroplastic surfing has been observed in the lab (Eeltink et al. 2023) and the field (Rainville et al. 2025); however, these studies each considered only one object type and were therefore unable to explore how an object's size, shape, and density relate to its surfing ability. Finally, the type of breaking wave is likely also important to surfing; breakers can be categorized into spillers, plungers, and surgers, and how these breaker types relate to object surfing is not clear.

3.1.3. Horizontal dispersion by waves. Beyond mean transport, waves can affect the horizontal dispersion of material. A wind-generated wave spectrum can be conceptualized as the superposition of many individual waves, each with its own Stokes drift. This distribution of Stokes drift velocities will cause particles to spread out diffusively as predicted by Herterich & Hasselmann (1982) using second-order wave theory, which was observed by Eeltink et al. (2023) in nonbreaking waves. Similarly, wave breaking can increase dispersion by enhancing horizontal transport variability; it can also lead to skewness in the dispersion, and a stochastic model has been proposed to capture this phenomenon, which models the wave-breaking surfing as jumps (Eeltink et al. 2023). We show examples of trajectories in nonbreaking waves and breaking waves in **Figure 4*b*,*c*** to demonstrate these jumps, which can be seen as sharp, localized increases in transport.

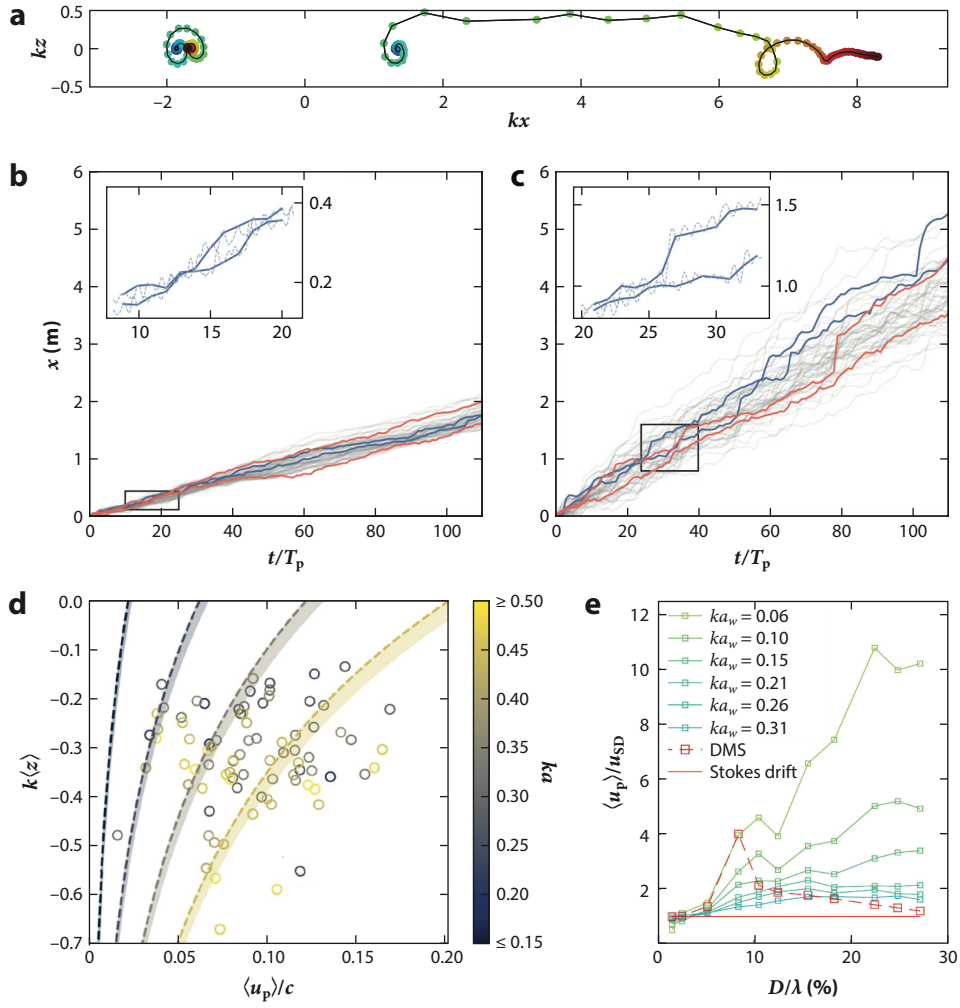

Figure 4

Observations of particles and objects drifting in waves. (*a*) Trajectories from simulation of a fluid particle under a (*left*) nonbreaking wave packet and (*right*) breaking wave packet. Color indicates time passing from blue to red. Panel adapted with permission from Deike et al. (2017). (*b*) Floating particle trajectories over time from experiments in irregular nonbreaking and (*c*) breaking waves. Experimental trajectories are shown in gray, wave-averaged experimental trajectories in blue, and simulated trajectories in orange. Panels *b* and *c* adapted from Eeltink et al. (2023) (CC BY 4.0). (*d*) Predicted Stokes drift (*dashed line*) and predicted enhancement effect (*shaded area*) from DiBenedetto et al. (2022) for bubbles. Data points indicate observed drift of bubbles generated under a breaking wave from laboratory experiments. Panel adapted with permission from Ruth et al. (2022). (*e*) Measured enhanced drift of finite-sized floating objects in waves. Green squares denote experimental data. The dashed red line is the theory for diffraction-modified Stokes drift (DMS) using the boundary element method to account for radiation and diffraction. The solid red line shows the Stokes drift of a fluid parcel. Panel adapted from Xiao et al. (2025) (CC BY 4.0).

If we consider the unaveraged wave field, it is clear the wave orbital motion induces unsteady straining in the flow that could potentially affect diffusion of material, although it has historically been neglected (Law 2000). Newer work shows that nonbreaking waves can distort the diffusion, e.g., causing an initially isotropic diffusivity to become anisotropic once wave-averaged

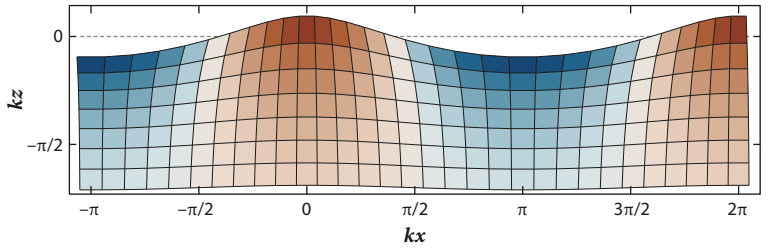

Figure 5

Fluid parcel deformation due to wave orbital motion. Color represents the vertical component of strain. Figure adapted from A. Russell & M. DiBenedetto (manuscript in preparation).

(A. Russell & M. DiBenedetto, manuscript in preparation). This effect is analogous to Stokes drift: Because fluid particles oversample the wave crests, they will spend more time in a vertically stretched and horizontally compressed configuration, as depicted in **Figure 5**. This will ultimately enhance horizontal diffusion and decrease vertical diffusion, an effect that is strongest near the surface and under steeper waves. While this unsteady strain has been considered in the context of wave–turbulence interactions (Teixeira & Belcher 2002, Guo & Shen 2013), its effects on diffusive transport have only recently been described.

3.1.4. Effects of particle shape and size on dispersion in waves. Particle size and shape have also been shown to affect how particles interact with and disperse in waves. For example, a set of analytical and numerical studies considered nonspherical particles settling in waves, finding that nonspherical particle dispersion is enhanced by the orientation-dependent drag coefficient (DiBenedetto et al. 2018, Pujara & Thiffeault 2023, Sunberg et al. 2024). These studies were limited to point particles in Stokes flow, and thus the dispersion effects were relatively small. However, one set of laboratory experiments with intermediate-sized particles ($Re_p = 110$–330) found that particle shape and size did impact dispersion in a measurable way (Clark et al. 2023). The study first showed how nonbreaking waves alone can increase particle dispersion relative to a unidirectional current (in some cases over a 300% increase). Next, they showed how not all the particles were equally affected by the waves, reporting that the particle Archimedes number was inversely related to particle dispersion in waves; i.e., larger particles were less affected by the waves.

3.2. Particles in Turbulence at the Ocean Surface

In addition to waves, surface turbulence will affect microplastics transport. Buoyant particles stay at or near the free surface, constraining how they interact with the turbulence.

3.2.1. Particle clustering at the ocean surface. While flow in the ocean is three-dimensional and incompressible, buoyant particles constrained to the free surface will experience a two-dimensional compressible flow. Thus, buoyant microplastics will preferentially concentrate in areas of surface convergence, which occurs over a range of scales. For example, large-scale convergence by the ocean circulation in the subtropical gyres can accumulate plastic (van Sebille et al. 2015), while at the submesoscale, convergent flow accumulates material at density fronts (D'Asaro et al. 2018, Taylor 2018). Langmuir turbulence (McWilliams et al. 1997) accumulates particles in windrows, and at the smallest scales, convergence generated by small-scale turbulence will also cluster particles (Li et al. 2025). Beyond surface convergence, studies showed that under convection, surface particles will preferentially concentrate in vortices (Chor et al. 2018) with a bias toward cyclonic convective vortices due to their low-pressure core (Dingwall et al. 2023); similar observations were made for small-scale vortices in free surface turbulence (Li et al. 2025).

Archimedes number: ratio of gravitational to viscous effects for particles in a fluid flow

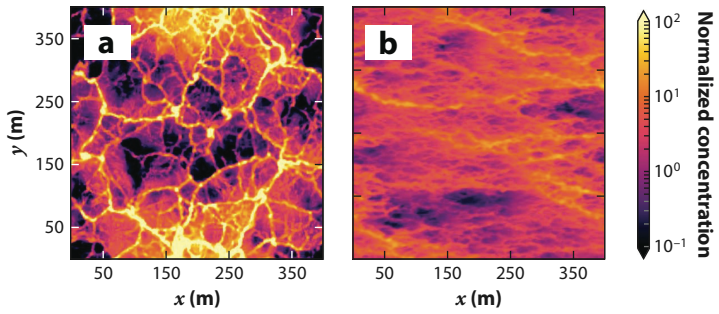

Figure 6

Surface particle concentration from large eddy simulation of the ocean mixed layer with buoyant particles. (*a*) Convection-dominated flow. (*b*) Flow dominated by Langmuir turbulence. Figure adapted with permission from Chor et al. (2018b).

This array of mechanisms produces locally high concentrations of plastic debris at many scales. We show examples from large eddy simulation (LES) of particle surface clustering under both convection and Langmuir turbulence in **Figure 6** (Chor et al. 2018b), which illustrates some of the expected clustering patterns. For example, convection-dominated flows form cell patterns, whereas Langmuir turbulence causes streaks.

3.2.2. Particle transport and dispersion at the ocean surface. Beyond clustering buoyant particles, surface turbulence also affects their transport. For example, Langmuir circulation can increase horizontal transport of buoyant material by preferentially accumulating it in areas of strong horizontal velocity (Kukulka 2020). Surface turbulence will also contribute to the dispersion of particles; this has been investigated experimentally in both channel flow and isotropic turbulence (Sanness Salmon et al. 2023, Li et al. 2024). Overall, particle kinematics are closely tied to the three-dimensional turbulence statistics beneath the surface. Particle pair dispersion rates tend to agree with Richardson–Obukhov theory, with some differences due to the surface compressibility (Schumacher & Eckhardt 2002, Li et al. 2024).

4. VERTICAL TRANSPORT NEAR THE OCEAN SURFACE

The vertical distribution of microplastics is inherently linked to plastic fate and transport. For example, a model of vertical concentration is needed to predict horizontal transport in vertically sheared ocean currents or to quantify microplastic exposure to sunlight (which decays with depth). The vertical concentration profile is also key to observations, enabling extrapolation of surface measurements to full water column plastic counts. From another perspective, measurements of microplastic vertical profiles may be leveraged to infer ocean vertical mixing, although this application has not yet been validated.

4.1. Vertical Concentration

Microplastic concentration is often modeled as an Eulerian concentration field. Consider the conservation equation for particle concentration c and particle velocity field $\mathbf{u}_\mathrm{p}$ with no sources or sinks,

$$\frac{\partial c}{\partial t} = -\nabla \cdot (\mathbf{u}_\mathrm{p} c)\,. \qquad 7.$$

We can decompose the quantities into a horizontal average and a fluctuation (e.g., $c = \langle c \rangle + c'$) and average the full equation, producing

$$\frac{\partial \langle c \rangle}{\partial t} = -\frac{\partial}{\partial z}\left(\langle w_\mathrm{p} \rangle \langle c \rangle + \langle w_\mathrm{p}' c' \rangle \right), \quad 8.$$

where the right-hand side terms represent the mean and turbulent vertical fluxes, respectively. To eliminate the left-hand side, we can assume that the concentration field is in a steady state. Next, we can assume an eddy diffusivity model for the turbulent particle flux: $\langle w_\mathrm{p}' c' \rangle = -K(z)\frac{\partial \langle c \rangle}{\partial z}$, where $K(z)$ is the eddy diffusivity profile. Integrating vertically and invoking surface boundary conditions of no-flux and a constant surface concentration $\langle c \rangle(z = 0) = c_0$, we find the following expression for the mean concentration profile:

$$\langle c \rangle(z) = c_0 \exp\left(\int_z^0 -\frac{\langle w_\mathrm{p} \rangle}{K(\zeta)} \mathrm{d}\zeta \right). \quad 9.$$

While the mean particle velocity can vary over depth, it is typically assumed to be the particle terminal rise velocity w_t (which is a function of particle size, shape, and density). We can also assume a constant diffusivity K_0 to further simplify the equation:

$$\langle c \rangle(z) = c_0 \exp(z w_\mathrm{t}/K_0). \quad 10.$$

Equation 10 is one of the most widely used models to account for wind-mixing effects on ocean surface microplastic measurements (Kukulka et al. 2012). Even though it is based on perhaps restrictive assumptions, its utility lies in its simplicity: The profile can be characterized by a single mixing length scale $L_\mathrm{m} = K_0/w_\mathrm{t}$. However, the simplifying assumption of a constant eddy diffusivity can be inappropriate, particularly when L_m approaches or exceeds the mixed layer depth, as may occur for small microplastics with small w_t (Poulain et al. 2019). This model also assumes that the microplastic vertical mixing is well-described by diffusive processes, which is not necessarily the case, e.g., in Langmuir turbulence.

By balancing particle buoyancy and turbulent mixing, the model in Equation 9 mirrors the Rouse profile used for sediment transport in open channel flow. It follows that the relevant nondimensional number for this balance is the Rouse number Z, which is a ratio of the rise/settling velocity of the particles to a relevant turbulent velocity scale. The Rouse number for a boundary layer flow can be defined as $Z = w_\mathrm{t}/u_*$, where u_* is the water friction velocity; in the sediment literature, the von Kármán constant and the turbulent Schmidt number Sc_t are often also included, but Sc_t is often assumed to be unity (we revisit that assumption later). At the ocean surface, this number has been referred to as the floatability parameter, which instead of the friction velocity uses w_*, which is a characteristic vertical fluid velocity that is a function of the wind shear, Stokes drift, and buoyancy flux (Chor et al. 2018b). The Rouse number is also similar to the settling velocity parameter for particles in turbulence, which uses the Kolmogorov velocity u_η as the relevant fluid velocity (Bec et al. 2024).

No matter the form of the Rouse number used, it can be applied to delineate clear regimes for buoyant particles. For $Z \ll 1$, turbulence is much stronger than particle buoyancy, and the particles become vertically well-mixed. For $Z \gg 1$, particle buoyancy is much stronger than turbulence, and we expect particles to stay trapped at the surface. Between these limits where $Z \sim 1$, both particle buoyancy and turbulence are important to the dynamics and the particles will partially disperse throughout the water column. We expect all of these regimes to exist at the ocean surface. For example, **Figure 7** plots observations of microplastic concentration from the Pacific Ocean; w_t was measured for each microplastic collected so that Z could be estimated directly. From the data, we clearly see that low Z corresponds to a well-mixed profile, high Z has most of the particles at the surface, and intermediate Z exhibits decay of the concentration profile with depth.

Rouse number: $Z = w_\mathrm{t}/u_*$; ratio of particle settling/rise velocity to friction velocity traditionally used in sediment transport

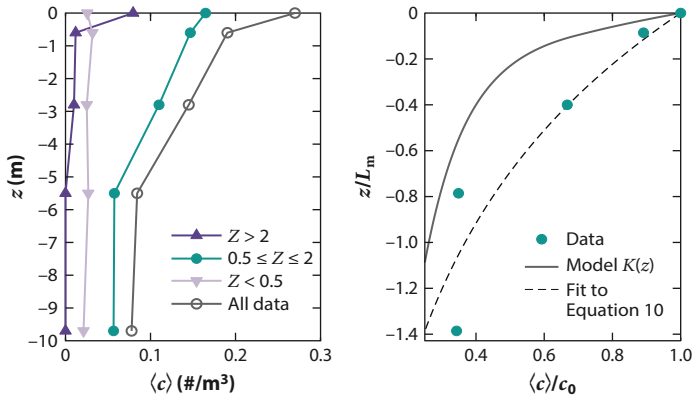

Figure 7

Observations of microplastic concentration as a function of depth. (*Left*) Profiles are plotted separately for different Z regimes. (*Right*) Partially mixed regime ($0.5 \leq Z \leq 2$) data (*circles*) plotted with modeled concentration profile using depth profile of diffusivity $K(z)$ using Brunner et al.'s (2015) parameterization (*solid line*) and a fit to Equation 10 using a constant K_0 and w_t (*dashed line*). The vertical axis is normalized by $L_m = K_0/w_t$. Figure adapted from DiBenedetto et al. (2023) (CC BY 4.0).

4.2. Vertical Mixing

This section summarizes recent work relevant to understanding and modeling the vertical mixing or dispersal of microplastics at the ocean surface.

4.2.1. Vertical mixing in large eddy simulations. When studying the dynamics of the ocean mixed layer, LES is a common tool. Resolving ocean dynamics over depths of $\mathcal{O}(100)$ m, LES has been used to develop new microplastic diffusivity parameterizations to account for the effects of Langmuir turbulence, breaking waves, and convection (Brunner et al. 2015, Kukulka et al. 2016, Chor et al. 2018b, Liang et al. 2018). However, LES does not typically resolve small-scale turbulence, wave-phase variability, wave–turbulence interactions, or particle–fluid interactions; rather, these processes are included in subgrid-scale models. For more information, readers are referred to the review article by Chamecki et al. (2019), which summarizes recent advances in studying the transport of material at the ocean surface with LES.

Brunner et al. (2015) developed microplastic diffusivity parameterizations using LES that resolved Langmuir turbulence and included effects from breaking waves. Their models tended to agree with microplastic observations. In those comparisons, however, they used the microplastic rise velocity w_t as a fitting parameter, which varied across their observations. In contrast, we again consider the study that measured w_t of each particle collected from a vertical profile in the open ocean (DiBenedetto et al. 2023). Applying Brunner et al.'s (2015) $K(z)$ model to these data (restricted to microplastics with $w_t \approx 1$ cm/s such that $Z \approx 1$), we see that the concentration is underpredicted at depth (right side of **Figure 7**), suggesting that the modeled diffusivity is too low. However, this analysis assumes that the relevant rise velocity is the terminal rise velocity, when in reality the rise velocity may be altered by the flow (see Section 4.3). Ultimately, this combined uncertainty in turbulent diffusivity (and nondiffusive transport) and microplastic rise velocities poses an ongoing challenge to accurately predicting vertical concentration profiles.

4.2.2. Turbulent diffusivity of microplastics. The turbulent dispersion of finite-sized particles is not necessarily the same as that of fluid particles. To compare the two, we consider the turbulent Schmidt number $Sc_t = \nu_t/K$, which is the ratio of the turbulent momentum diffusivity

ν_t to turbulent particle diffusivity K. For microplastics (as with sediment), Sc_t is often assumed to be unity (Kukulka & Brunner 2015, Onink et al. 2022), yet measuring it directly can be difficult. Various sediment studies estimated diffusivity by combining mean concentration profiles with an assumed settling velocity, finding $Sc_t < 1$ (Lyn 2008). In contrast, Chauchat et al. (2022) found $Sc_t \approx 3 - 4$ by directly calculating the turbulent sediment flux. They also found that the settling velocity of their particles was reduced relative to the terminal settling velocity, emphasizing that unverified assumptions about rise/settling velocity may cause errors in diffusivity estimates.

There are a variety of mechanisms that can cause Sc_t to deviate from unity for finite-sized particles. One common example is the crossing trajectories effect (Csanady 1963, Berk & Coletti 2021). Recall that diffusivity scales with the Lagrangian integral timescale and the velocity fluctuation squared (Taylor 1922). As microplastics rise/settle due to gravity and cross fluid trajectories, their velocity signal will decorrelate more quickly than that of an equivalent fluid particle, resulting in a lower integral timescale and lower diffusivity ($Sc_t > 1$). Particle inertia can also affect diffusivity; e.g., inertia can increase the temporal autocorrelation of the particle motion, thereby increasing diffusivity of the particles ($Sc_t < 1$) (Squires & Eaton 1991, Machicoane & Volk 2016). These topics are active areas of research in the particle-laden turbulence community, often studied for small, spherical particles that are much heavier than the carrier fluid (Brandt & Coletti 2022). With respect to microplastics, it remains to be seen how near-neutral buoyancy, particle shape, and small to intermediate size affect turbulent dispersion, although experiments have started to shed light on these processes (e.g., Baker & Coletti 2022, Giurgiu et al. 2024).

4.2.3. Wave effects on vertical mixing. Nonbreaking waves can affect the distribution of buoyant particles. For example, phase-varying strain leads to phase-varying stretching and squashing of the vertical concentration distribution. Under wave crests, particles can be mixed lower relative to the instantaneous free surface due to vertical divergence in the flow field, whereas under the troughs, particles will stay closer to the free surface due to vertical convergence (DiBenedetto et al. 2022). Nonbreaking waves can also generate turbulence and mixing directly (Qiao et al. 2004, Babanin & Haus 2009), while breaking waves generate turbulence that further enhances mixing near the ocean surface (Perlin et al. 2013).

Waves also affect the vertical transport of microplastics through their generation of Langmuir circulation, which arises from the interaction between winds and waves. Under strong winds, Langmuir circulation cells can become more irregular, referred to as Langmuir turbulence, which is characterized by strong downward jets that can inject buoyant surface particles into the mixed layer below (Kukulka & Brunner 2015). The tendency for Langmuir circulation to preferentially concentrate buoyant material (as seen in **Figure 6*b***) can also complicate mixing predictions. For example, turbulent kinetic energy from breaking waves was observed to be elevated under windrows (Zippel et al. 2020, Fisher & Nidzieko 2024), which could further enhance particle mixing.

4.3. Rise Velocity

Particle rise velocity is a key component of buoyant particle behavior at the free surface. To reveal the processes that control rise velocity, we decompose a particle's velocity $\mathbf{u}_p$ into two components: the fluid velocity $\mathbf{u}_f$ at the location of the particle and the slip (or relative) velocity $\mathbf{u}_p - \mathbf{u}_f$; this decomposition gives $\mathbf{u}_p = (\mathbf{u}_f) + (\mathbf{u}_p - \mathbf{u}_f)$. In quiescent flow, the particle's vertical slip velocity (in steady state) is equivalent to the terminal velocity $w_p - w_f = w_t$. An unsteady flow field can cause a particle's average rise velocity to deviate from its quiescent value. For a spherical particle, this can occur because of (*a*) a change in the mean fluid velocity the particle encounters such that $\langle w_f \rangle \neq 0$ due to preferential sampling and/or (*b*) a change in the particle's mean slip velocity

$\langle w_p - w_f \rangle \neq w_t$, which can be due to unsteady forces on the particle. Nonspherical particles will have additional orientation-dependent effects due to their anisotropic drag coefficient. Note that while the particle rise velocity does mirror the particle settling velocity, the dynamics are not exactly symmetric because a buoyant particle has less inertia than a heavy particle.

4.3.1. Effects on the slip velocity of microplastics. The drag force on a particle is a function of the particle Reynolds number, defined here with the slip velocity and particle diameter: $Re_p = |\mathbf{u}_p - \mathbf{u}_f| d_p/\nu$. For $Re_p \ll 1$, the drag force is linear with slip velocity, while for $Re_p > 1$, the drag force becomes a nonlinear function of slip velocity. The result of this nonlinearity is that increased absolute slip in the horizontal direction due to fluid fluctuations increases the total drag force, which in turn requires a reduction in the vertical slip velocity to balance gravity and buoyancy. In turbulence, this nonlinear drag effect reduces the average vertical slip velocity, thereby reducing the overall rise (settling) velocity of buoyant (heavy) particles (Good et al. 2014, Ruth et al. 2021, Liu et al. 2024). Similar reductions have been predicted for particles settling in wavy flows, although not explicitly observed (Nielsen 1984, Hwang 1990).

As particle size increases, other forces become increasingly important. For example, the Basset history force (Guseva et al. 2016, Li et al. 2023) and the added (or virtual) mass force can also reduce the overall slip velocity (Li et al. 2023). These reductions have been observed for settling particles in turbulent flows relevant to the ocean, so we expect them to also be relevant to buoyant microplastics.

4.3.2. Preferential sampling in waves. Surface waves generate no mean vertical flow. Yet nonfluid particles can preferentially sample the flow, producing a net vertical effect. As particles rise (settle) under waves, they will oversample the upward (downward) part of the wave orbital, enhancing their net transport. This can be thought of as a vertical Stokes drift and was first described by Santamaria et al. (2013) for particles with Stokes drag in deep water waves and later expanded to particles with nonlinear drag in finite water depth by DiBenedetto et al. (2022). This effect is purely kinematic. However, particle inertia can further affect this enhancement by altering the orbital motion of the particles. Laboratory observations of heavy spherical particles settling under waves found up to a 20% increase in settling velocity near the surface due to preferential sampling (Clark et al. 2020), an effect that is larger than the increase predicted by theory. Analogous experiments with rising particles have yet to be conducted.

4.3.3. Preferential sampling in turbulence. Preferential sampling of particles in turbulence is a well-documented effect for heavy particles with $St \sim 1$ (Balachandar & Eaton 2010). These inertial particles exhibit enhanced settling velocities due to a process known as fast-tracking where they preferentially accumulate in areas with downward velocity and low vorticity (Wang & Maxey 1993, Aliseda et al. 2002, Good et al. 2014). The corresponding behavior for positively buoyant particles is less well-documented (Mathai et al. 2020). Most studies have focused on bubbles ($\rho_p/\rho_f \approx 0$). While some have observed a reduction in rise velocity for bubbles due to preferential concentration in regions of downwelling and high vorticity (Poorte & Biesheuvel 2002, Mazzitelli & Lohse 2004, Aliseda & Lasheras 2011), others observed little preferential sampling (Ruth et al. 2021, Liu et al. 2024). However, one experimental study of near-neutrally buoyant oil droplets ($\rho_p/\rho_f = 0.85$) observed an increase in rise velocity in turbulence by up to a factor of six (Friedman & Katz 2002). This result demonstrates that rise velocity enhancement due to preferential sampling is possible in turbulence, and it is potentially enabled by near-neutral buoyancy and added mass (Marchioli et al. 2007).

4.3.4. Effects from particle anisotropy. Anisotropic particles are characterized by their orientation-dependent drag coefficients and lift forces. This means that much of the effect on their

net rise (and settling) velocity comes from their orientation behavior in a particular fluid flow. We focus specifically on work done in waves and refer readers to other sources for information on nonspherical particles in turbulence (Voth & Soldati 2017).

Numerical and analytical work showed that waves induce a preferential orientation of inertialess particles (DiBenedetto & Ouellette 2018, DiBenedetto et al. 2018), an effect that can be conceptualized as an angular analog to Stokes drift. This preferential orientation aligns the symmetry axis of the particles with the direction of wave propagation and tends to align the particles such that their vertical drag coefficient approaches its maximum, especially for the most anisotropic particles. This will reduce rise/settling velocities relative to a randomly orienting particle. As particles become more inertial, this wave-induced preferential orientation can break down (DiBenedetto et al. 2019).

5. TRANSPORT AT BOUNDARIES

5.1. Entrainment of Particles from the Surface to the Subsurface

Entrainment is defined in this context as the process by which particles at the free surface become fully submerged into the subsurface flow. Conceptually, this parallels erosion and resuspension at a solid boundary and occurs when entraining forces overcome the buoyancy and surface tension that hold a particle at the surface. Buoyancy is most important for larger particles, but surface tension can become dominant for small particles.

While studies have examined the drawdown of floating particulate in stirred tanks (Khazam & Kresta 2008), much less research has been conducted on solid particle entrainment in the ocean, though the relevant physical processes are likely similar to those responsible for more widely studied phenomena of air and oil entrainment (Li et al. 2017, Deike 2022). For example, air can be entrained into the subsurface by breaking waves, which transport mass and momentum downward; this is likely a dominant mechanism for particle entrainment as well. Additionally, short waves can exhibit microbreaking with no air entrainment, though they create surface convergent flows (Peirson & Banner 2003) that could potentially entrain solid particles. Beyond breaking waves, particles may be entrained from vortices aligned normal to the free surface and downward velocity associated with strong surface convergence, as discussed in Section 3.2.1.

Despite the parallels to air entrainment, microplastics can have nonnegligible inertia that affects their behavior. Moreover, air bubbles are generated and destroyed by fluid processes (Chan et al. 2021, Ni 2024), whereas solid particles maintain a stable form; therefore, we cannot apply existing air entrainment models to solid particles without modifications. Another key difference is that breaking waves always have access to entrainable air, whereas particles may not be uniformly distributed with respect to the breaking waves. Thus, any bias in how floating particles sample waves would affect their likelihood of being entrained during breaking. These complications have yet to be studied in detail, but they must be addressed in order to apply existing entrainment models to microplastics.

Finally, surface tension is important at the free surface when $d_p/\lambda_c < 1$. Nearby particles can cluster together on a surface, as reviewed by Protière (2023). In a standing wave, this capillary force can cause particles to preferentially accumulate into the nodes and antinodes (Falkovich et al. 2005).

5.2. Transfer of Particles from the Ocean to the Atmosphere

Beyond the ocean, microplastics also pollute the atmosphere (Brahney et al. 2021). The ocean can contribute to atmospheric microplastics via sea spray. Sea spray droplets can be formed either from bubbles bursting at the surface or from wind stress applied to waves (known as spume droplets)

(Veron 2015, Deike 2022). Both mechanisms can transport microplastics into the atmosphere, although the spume droplet mechanism may be less effective because high wind stress will also generate strong mixing of microplastics away from the free surface. In contrast, before the bubbles burst, they rise through the water column where they can scavenge microplastics (Dubitsky et al. 2023, Shaw et al. 2023). When these bubbles hit the free surface and pop, they can generate enriched jet drops that have relatively high levels of microplastics (Ji et al. 2022, Dubitsky et al. 2023).

Beaching: defined here as when a particle is left behind on the beach after the water has receded

5.3. Transport on Beaches

Coastlines represent boundary conditions between the land and ocean, controlling how plastic is transported between the two; they are also a major reservoir of plastic debris (Lebreton et al. 2019, Onink et al. 2021). Transport processes in this nearshore region are especially complex, and readers are referred to a recent review (Moulton et al. 2023) for more information. This review specifically focuses on transport on beaches. Short of direct observations, no methods currently exist to predict a priori the extent to which an individual beach may trap and store plastic. This speaks to the complexity of the dynamics at play, which depend on hydrodynamics, beach composition (e.g., sand grain size, beach slope), and the properties of the plastic particles themselves.

The swash zone is the region where ocean waves run up and down a beach after they break in the surf zone. Swash dynamics are key to predicting sediment transport (Masselink & Puleo 2006) and are therefore also important to the transport of plastic pollution. Most work on plastic transport in the swash zone has been from laboratory experiments, with results showing generally that more buoyant (lower density) particles are more likely to beach (e.g., Forsberg et al. 2020, Kerpen et al. 2020, Larsen et al. 2023, Núñez et al. 2023). These experiments were carried out in wave tanks and all included transport in nonbreaking waves, breaking waves in the surf zone, and the swash zone, so it was not always possible to isolate the relevant transport processes in each regime.

Some studies have tried to precisely examine buoyant particle interactions with the swash. Davidson et al. (2023) developed a model of particle motion in the swash using a modified Maxey–Riley–Gatignol equation and a ballistic swash flow model. Their model, validated by laboratory experiments, described two parameters important to the particle transport: initial position in the swash flow and *St*. They found that for particles that initially started in the water, higher-*St* (more inertial) particles were more likely to remain on the beach after flow reversal, thus increasing their beaching likelihood and final position on the beach, as shown in **Figure 8**. Another study

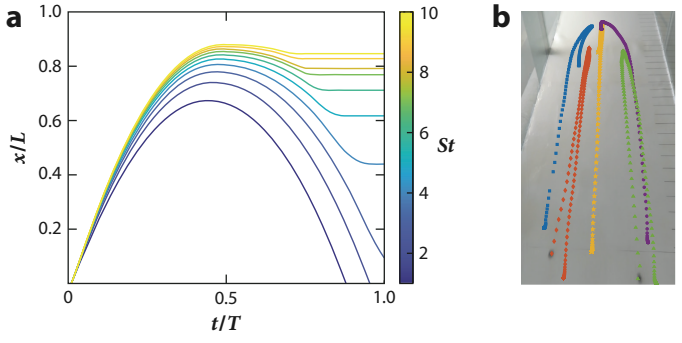

Figure 8

Particle trajectories in the swash zone. (*a*) Simulated cross-shore position of inertial particles over time with varying *St*. Cross-shore position *x* is normalized by run-up length *L*, and time *t* is normalized by the swash period *T*. Higher-*St* particles become beached. (*b*) Trajectories of particles in a laboratory swash flow. Figure adapted from Davidson et al. (2023) (CC BY 4.0).

has focused on swash flow transport of particles starting on the beach rather than in the water (C. Abarca, T. Ling & M. DiBenedetto, manuscript in preparation). The authors found a contrasting result: More inertial particles with higher *St* were more likely to leave the beach in a swash event. This was attributed to the fact that higher *St* caused a larger lag when the particle was initially picked up by the wave, keeping it further back from the swash front and enabling offshore transport in the backwash. These two studies highlight the complexities of studying buoyant particles in the swash zone and that both particle properties and initial conditions affect fate and transport.

SUMMARY POINTS

1. Microplastics in the ocean are unique among ocean particles due to their near-neutral buoyancy and diverse array of shapes. They tend to fall within an intermediate particle Reynolds number regime, and their dynamics are often affected by their finite size.
2. Microplastic and macroplastic research has revealed nontrivial particle–wave interactions that can enhance both their vertical and horizontal transport and dispersion at the ocean surface.
3. Estimating the vertical distribution of ocean microplastics requires properly predicting both the rise velocity and the turbulent mixing of microplastics. However, both the rise velocity and turbulent diffusivity can be coupled to the particle and flow properties, making them difficult to predict in tandem.
4. Transport across ocean boundaries, including on beaches and at the air–sea interface, represents critical but poorly understood processes in the overall plastic budget.

FUTURE ISSUES

1. Microplastics are heterogeneous in form. While this review focused mainly on larger particles where finite size is important to the fluid dynamics, the smallest microplastics are potentially the most damaging to human health. Transport properties will vary across this range of scales, and therefore understanding how microplastic particle size distributions evolve in the environment is necessary to characterize their impact as a pollutant.
2. Our understanding of microplastic transport in the ocean is impeded by noisy and sparse in situ observations. Future efforts should focus on collecting consistent and high-density measurements of microplastics concentrations and properties, including below the ocean surface.
3. Transport of microplastics between ocean reservoirs, e.g., sea ice, biology, marine sediments, and the deep sea, is an important area of research needed to close the ocean plastic budget.
4. Microplastic fate and transport is mediated by interactions and aggregation with bubbles and environmental particles, such as sediments and biological materials. Understanding these processes requires interdisciplinary research.
5. Ocean surface dynamics under realistic conditions should be further explored, including the complexities introduced when particles interact with surfactants, breaking waves, and foam.

DISCLOSURE STATEMENT

The author is not aware of any affiliations, memberships, funding, or financial holdings that might be perceived as affecting the objectivity of this review.

ACKNOWLEDGMENTS

I thank Matt Hoffman and Luc Deike for helpful discussion and feedback in the preparation of this review. This work has been supported by National Science Foundation CAREER award 2237550 to M.H.D.

LITERATURE CITED

Aliseda A, Cartellier A, Hainaux F, Lasheras JC. 2002. Effect of preferential concentration on the settling velocity of heavy particles in homogeneous isotropic turbulence. *J. Fluid Mech.* 468:77–105

Aliseda A, Lasheras JC. 2011. Preferential concentration and rise velocity reduction of bubbles immersed in a homogeneous and isotropic turbulent flow. *Phys. Fluids* 23(9):093301

Andrady AL. 2017. The plastic in microplastics: a review. *Mar. Pollut. Bull.* 119(1):12–22

Andrady AL, Koongolla B. 2022. Degradation and fragmentation of microplastics. In *Plastics and the Ocean*, ed. AL Andrady. Wiley. 1st ed.

Angle BR, Rau MJ, Byron ML. 2024. Settling of nonuniform cylinders at intermediate Reynolds numbers. *Phys. Rev. Fluids* 9(7):070501

Babanin AV, Haus BK. 2009. On the existence of water turbulence induced by nonbreaking surface waves. *J. Phys. Oceanogr.* 39(10):2675–79

Baker LJ, Coletti F. 2022. Experimental investigation of inertial fibres and disks in a turbulent boundary layer. *J. Fluid Mech.* 943:A27

Balachandar S, Eaton JK. 2010. Turbulent dispersed multiphase flow. *Annu. Rev. Fluid Mech.* 42:111–33

Barrows APW, Neumann CA, Berger ML, Shaw SD. 2017. Grab vs. neuston tow net: a microplastic sampling performance comparison and possible advances in the field. *Anal. Methods* 9(9):1446–53

Bec J, Gustavsson K, Mehlig B. 2024. Statistical models for the dynamics of heavy particles in turbulence. *Annu. Rev. Fluid Mech.* 56:189–213

Berk T, Coletti F. 2021. Dynamics of small heavy particles in homogeneous turbulence: a Lagrangian experimental study. *J. Fluid Mech.* 917:A47

Bond T, Ferrandiz-Mas V, Felipe-Sotelo M, van Sebille E. 2018. The occurrence and degradation of aquatic plastic litter based on polymer physicochemical properties: a review. *Crit. Rev. Environ. Sci. Technol.* 48(7–9):685–722

Borrelle SB, Ringma J, Law KL, Monnahan CC, Lebreton L, et al. 2020. Predicted growth in plastic waste exceeds efforts to mitigate plastic pollution. *Science* 369(6510):1515–18

Brahney J, Mahowald N, Prank M, Cornwell G, Klimont Z, et al. 2021. Constraining the atmospheric limb of the plastic cycle. *PNAS* 118(16):e2020719118

Brandt L, Coletti F. 2022. Particle-laden turbulence: progress and perspectives. *Annu. Rev. Fluid Mech.* 54:159–89

Brouzet C, Guiné R, Dalbe MJ, Favier B, Vandenberghe N, et al. 2021. Laboratory model for plastic fragmentation in the turbulent ocean. *Phys. Rev. Fluids* 6(2):024601

Brouzet C, Verhille G, Le Gal P. 2014. Flexible fiber in a turbulent flow: a macroscopic polymer. *Phys. Rev. Lett.* 112(7):074501

Brunner K, Kukulka T, Proskurowski G, Law KL. 2015. Passive buoyant tracers in the ocean surface boundary layer: 2. Observations and simulations of microplastic marine debris. *J. Geophys. Res. Oceans* 120(11):7559–73

Burd AB, Jackson GA. 2009. Particle aggregation. *Annu. Rev. Mar. Sci.* 1:65–90

Calvert R, McAllister M, Whittaker C, Raby A, Borthwick A, van den Bremer T. 2021. A mechanism for the increased wave-induced drift of floating marine litter. *J. Fluid Mech.* 915:A73

Calvert R, Mol J, Sutherland BR, van den Bremer TS. 2025. Attenuation of progressive surface gravity waves by floating spheres. *Sci. Rep.* 15(1):1770

Calvert R, Peytavin A, Pham Y, Duhamel A, van der Zanden J, et al. 2024. A laboratory study of the effects of size, density, and shape on the wave-induced transport of floating marine litter. *J. Geophys. Res. Oceans* 129(7):e2023JC020661

Carpenter EJ, Smith KL. 1972. Plastics on the Sargasso Sea surface. *Science* 175(4027):1240–41

Chamas A, Moon H, Zheng J, Qiu Y, Tabassum T, et al. 2020. Degradation rates of plastics in the environment. *ACS Sustainable Chem. Eng.* 8(9):3494–511

Chamecki M, Chor T, Yang D, Meneveau C. 2019. Material transport in the ocean mixed layer: recent developments enabled by large eddy simulations. *Rev. Geophys.* 57(4):1338–71

Chan WHR, Johnson PL, Moin P, Urzay J. 2021. The turbulent bubble break-up cascade. Part 2. Numerical simulations of breaking waves. *J. Fluid Mech.* 912:A43

Chauchat J, Hurther D, Revil-Baudard T, Cheng Z, Hsu TJ. 2022. Controversial turbulent Schmidt number value in particle-laden boundary layer flows. *Phys. Rev. Fluids* 7(1):014307

Chor T, Yang D, Meneveau C, Chamecki M. 2018a. Preferential concentration of noninertial buoyant particles in the ocean mixed layer under free convection. *Phys. Rev. Fluids* 3(6):064501

Chor T, Yang D, Meneveau C, Chamecki M. 2018b. A turbulence velocity scale for predicting the fate of buoyant materials in the oceanic mixed layer. *Geophys. Res. Lett.* 45(21):11817–26

Chubarenko I, Efimova I, Bagaeva M, Bagaev A, Isachenko I. 2020. On mechanical fragmentation of single-use plastics in the sea swash zone with different types of bottom sediments: insights from laboratory experiments. *Mar. Pollut. Bull.* 150:110726

Clark LK, DiBenedetto MH, Ouellette NT, Koseff JR. 2020. Settling of inertial nonspherical particles in wavy flow. *Phys. Rev. Fluids* 5(12):124301

Clark LK, DiBenedetto MH, Ouellette NT, Koseff JR. 2023. Dispersion of finite-size, non-spherical particles by waves and currents. *J. Fluid Mech.* 954:A3

Clift R, Grace JR, Weber ME. 2005. *Bubbles, Drops, and Particles*. Dover

Cohen JH, Internicola AM, Mason RA, Kukulka T. 2019. Observations and simulations of microplastic debris in a tide, wind, and freshwater-driven estuarine environment: the Delaware Bay. *Environ. Sci. Technol.* 53(24):14204–11

Colson BC, Michel APM. 2021. Flow-through quantification of microplastics using impedance spectroscopy. *ACS Sens.* 6(1):238–44

Cózar A, Arias M, Suaria G, Viejo J, Aliani S, et al. 2024. Proof of concept for a new sensor to monitor marine litter from space. *Nat. Commun.* 15(1):4637

Cózar A, Echevarría F, González-Gordillo JI, Irigoien X, Úbeda B, et al. 2014. Plastic debris in the open ocean. *PNAS* 111(28):10239–44

Cózar A, Sanz-Martín M, Martí E, González-Gordillo JI, Ubeda B, et al. 2015. Plastic accumulation in the Mediterranean Sea. *PLOS ONE* 10(4):e0121762

Csanady GT. 1963. Turbulent diffusion of heavy particles in the atmosphere. *J. Atmos. Sci.* 20(3):201–8

D'Asaro EA, Shcherbina AY, Klymak JM, Molemaker J, Novelli G, et al. 2018. Ocean convergence and the dispersion of flotsam. *PNAS* 115(6):1162–67

Davidson B, Brenner J, Pujara N. 2023. Beaching model for buoyant marine debris in bore-driven swash. *Flow* 3:E35

de Vos A, Aluwihare L, Youngs S, DiBenedetto MH, Ward CP, et al. 2021. The *M/V X-Press Pearl* nurdle spill: contamination of burnt plastic and unburnt nurdles along Sri Lanka's beaches. *ACS Environ. Au* 2:128–35

Deike L. 2022. Mass transfer at the ocean–atmosphere interface: the role of wave breaking, droplets, and bubbles. *Annu. Rev. Fluid Mech.* 54:191–224

Deike L, Pizzo N, Melville WK. 2017. Lagrangian transport by breaking surface waves. *J. Fluid Mech.* 829:364–91

DiBenedetto MH. 2020. Non-breaking wave effects on buoyant particle distributions. *Front. Mar. Sci.* 7:148

DiBenedetto MH, Clark LK, Pujara N. 2022. Enhanced settling and dispersion of inertial particles in surface waves. *J. Fluid Mech.* 936:A38

DiBenedetto MH, Donohue J, Tremblay K, Edson E, Law KL. 2023. Microplastics segregation by rise velocity at the ocean surface. *Environ. Res. Lett.* 18(2):024036
DiBenedetto MH, Koseff JR, Ouellette NT. 2019. Orientation dynamics of nonspherical particles under surface gravity waves. *Phys. Rev. Fluids* 4(3):034301
DiBenedetto MH, Ouellette NT. 2018. Preferential orientation of spheroidal particles in wavy flow. *J. Fluid Mech.* 856:850–69
DiBenedetto MH, Ouellette NT, Koseff JR. 2018. Transport of anisotropic particles under waves. *J. Fluid Mech.* 837:320–40
Dingwall J, Chor T, Taylor JR. 2023. Large eddy simulations of the accumulation of buoyant material in oceanic wind-driven and convective turbulence. *J. Fluid Mech.* 954:A27
Dubitsky L, McRae O, Bird JC. 2023. Enrichment of scavenged particles in jet drops determined by bubble size and particle position. *Phys. Rev. Lett.* 130(5):054001
Eeltink D, Calvert R, Swagemakers J, Xiao Q, van den Bremer T. 2023. Stochastic particle transport by deep-water irregular breaking waves. *J. Fluid Mech.* 971:A38
Eriksen M, Lebreton LCM, Carson HS, Thiel M, Moore CJ, et al. 2014. Plastic pollution in the world's oceans: more than 5 trillion plastic pieces weighing over 250,000 tons afloat at sea. *PLOS ONE* 9(12):e111913
Evans MC, Ruf CS. 2022. Toward the detection and imaging of ocean microplastics with a spaceborne radar. *IEEE Trans. Geosci. Remote Sens.* 60:4202709
Falkovich G, Weinberg A, Denissenko P, Lukaschuk S. 2005. Floater clustering in a standing wave. *Nature* 435(7045):1045–46
Fisher AW, Nidzieko NJ. 2024. AUV observations of Langmuir turbulence in a stratified shelf sea. *J. Phys. Oceanogr.* 54(9):1903–20
Forsberg PL, Sous D, Stocchino A, Chemin R. 2020. Behaviour of plastic litter in nearshore waters: first insights from wind and wave laboratory experiments. *Mar. Pollut. Bull.* 153:111023
Friedman PD, Katz J. 2002. Mean rise rate of droplets in isotropic turbulence. *Phys. Fluids* 14(9):3059–73
Fröhlich K, Meinke M, Schröder W. 2020. Correlations for inclined prolates based on highly resolved simulations. *J. Fluid Mech.* 901:A5
Fuchs HL, Gerbi GP. 2016. Seascape-level variation in turbulence- and wave-generated hydrodynamic signals experienced by plankton. *Progress Oceanogr.* 141:109–29
Gatignol R. 1983. The Faxén formulae for a rigid particle in an unsteady non-uniform Stokes flow. *J. Mec. Theor. Appl.* 2(2):143–60
Geyer R, Jambeck JR, Law KL. 2017. Production, use, and fate of all plastics ever made. *Sci. Adv.* 3(7):e1700782
Giurgiu V, Caridi GCA, De Paoli M, Soldati A. 2024. Full rotational dynamics of plastic microfibers in turbulence. *Phys. Rev. Lett.* 133(5):054101
Good GH, Ireland PJ, Bewley GP, Bodenschatz E, Collins LR, Warhaft Z. 2014. Settling regimes of inertial particles in isotropic turbulence. *J. Fluid Mech.* 759:R3
Guerrini F, Lobelle D, Mari L, Casagrandi R, van Sebille E. 2023. Modeling carbon export mediated by biofouled microplastics in the Mediterranean Sea. *Limnol. Oceanogr.* 68(5):1078–90
Guo X, Shen L. 2013. Numerical study of the effect of surface waves on turbulence underneath. Part 1. Mean flow and turbulence vorticity. *J. Fluid Mech.* 733:558–87
Guseva K, Daitche A, Feudel U, Tél T. 2016. History effects in the sedimentation of light aerosols in turbulence: the case of marine snow. *Phys. Rev. Fluids* 1(7):074203
Hartmann NB, Hüffer T, Thompson RC, Hassellöv M, Verschoor A, et al. 2019. Are we speaking the same language? Recommendations for a definition and categorization framework for plastic debris. *Environ. Sci. Technol.* 53(3):1039–47
Herterich K, Hasselmann K. 1982. The horizontal diffusion of tracers by surface waves. *J. Phys. Oceanogr.* 12(7):704–11
Huang G, Huang ZH, Law AWK. 2016. Analytical study on drift of small floating objects under regular waves. *J. Eng. Mech.* 142(6):06016002
Huang G, Law AWK, Huang Z. 2011. Wave-induced drift of small floating objects in regular waves. *Ocean Eng.* 38(4):712–18
Hwang PA. 1990. Velocity of particles falling in vertically oscillating flow. *J. Hydraul. Eng.* 116(1):23–35

Isobe A, Azuma T, Cordova MR, Cózar A, Galgani F, et al. 2021. A multilevel dataset of microplastic abundance in the world's upper ocean and the Laurentian Great Lakes. *Microplastics Nanoplastics* 1(1):16
Jambeck JR, Geyer R, Wilcox C, Siegler TR, Perryman M, et al. 2015. Plastic waste inputs from land into the ocean. *Science* 347(6223):768–71
Ji B, Singh A, Feng J. 2022. Water-to-air transfer of nano/microsized particulates: enrichment effect in bubble bursting jet drops. *Nano Lett.* 22(13):5626–34
Kaandorp MLA, Dijkstra HA, van Sebille E. 2021. Modelling size distributions of marine plastics under the influence of continuous cascading fragmentation. *Environ. Res. Lett.* 16(5):054075
Kaandorp MLA, Lobelle D, Kehl C, Dijkstra HA, van Sebille E. 2023. Global mass of buoyant marine plastics dominated by large long-lived debris. *Nat. Geosci.* 16(8):689–94
Kerpen NB, Schlurmann T, Schendel A, Gundlach J, Marquard D, Hüpgen M. 2020. Wave-induced distribution of microplastic in the surf zone. *Front. Mar. Sci.* 7:590565
Khazam O, Kresta SM. 2008. Mechanisms of solids drawdown in stirred tanks. *Can. J. Chem. Eng.* 86(4):622–34
Kooi M, Koelmans AA. 2019. Simplifying microplastic via continuous probability distributions for size, shape, and density. *Environ. Sci. Technol. Lett.* 6(9):551–57
Kooi M, Nes EHV, Scheffer M, Koelmans AA. 2017. Ups and downs in the ocean: effects of biofouling on vertical transport of microplastics. *Environ. Sci. Technol.* 51(14):7963–71
Kukulka T. 2020. Horizontal transport of buoyant material by turbulent jets in the upper ocean. *J. Phys. Oceanogr.* 50(3):827–43
Kukulka T, Brunner K. 2015. Passive buoyant tracers in the ocean surface boundary layer: 1. Influence of equilibrium wind-waves on vertical distributions. *J. Geophys. Res. Oceans* 120(5):3837–58
Kukulka T, Law KL, Proskurowski G. 2016. Evidence for the influence of surface heat fluxes on turbulent mixing of microplastic marine debris. *J. Phys. Oceanogr.* 46(3):809–15
Kukulka T, Proskurowski G, Morét-Ferguson S, Meyer DW, Law KL. 2012. The effect of wind mixing on the vertical distribution of buoyant plastic debris. *Geophys. Res. Lett.* 39(7):2012GL051116
Landrigan PJ, Raps H, Cropper M, Bald C, Brunner M, et al. 2023. The Minderoo-Monaco Commission on Plastics and Human Health. *Ann. Glob. Health* 89(1):23
Larsen BE, Al-Obaidi MAA, Guler HG, Carstensen S, Goral KD, et al. 2023. Experimental investigation on the nearshore transport of buoyant microplastic particles. *Mar. Pollut. Bull.* 187:114610
Lau WWY, Shiran Y, Bailey RM, Cook E, Stuchtey MR, et al. 2020. Evaluating scenarios toward zero plastic pollution. *Science* 369(6510):1455–61
Law AW. 2000. Taylor dispersion of contaminants due to surface waves. *J. Hydraulic Res.* 38(1):41–48
Law KL. 2017. Plastics in the marine environment. *Annu. Rev. Mar. Sci.* 9:205–29
Law KL, Morét-Ferguson S, Maximenko NA, Proskurowski G, Peacock EE, et al. 2010. Plastic accumulation in the North Atlantic subtropical gyre. *Science* 329(5996):1185–88
Lebreton L, Egger M, Slat B. 2019. A global mass budget for positively buoyant macroplastic debris in the ocean. *Sci. Rep.* 9(1):12922
Li C, Miller J, Wang J, Koley SS, Katz J. 2017. Size distribution and dispersion of droplets generated by impingement of breaking waves on oil slicks. *J. Geophys. Res. Oceans* 122(10):7938–57
Li S, Bragg AD, Katul G. 2023. Reduced sediment settling in turbulent flows due to Basset history and virtual mass effects. *Geophys. Res. Lett.* 50(22):e2023GL105810
Li Y, Salmon HS, Hassaini R, Chang K, Mucignat C, Coletti F. 2025. Spatiotemporal scales of motion and particle clustering in free-surface turbulence. *Phys. Rev. Fluids* 10(3):034602
Li Y, Wang Y, Qi Y, Coletti F. 2024. Relative dispersion in free-surface turbulence. *J. Fluid Mech.* 993:R2
Liang JH, Wan X, Rose KA, Sullivan PP, McWilliams JC. 2018. Horizontal dispersion of buoyant materials in the ocean surface boundary layer. *J. Phys. Oceanogr.* 48(9):2103–25
Lick W, Huang H, Jepsen R. 1993. Flocculation of fine-grained sediments due to differential settling. *J. Geophys. Res. Oceans* 98(C6):10279–88
Liu Z, Farsoiya PK, Perrard S, Deike L. 2024. Direct numerical simulation of bubble rising in turbulence. *J. Fluid Mech.* 999:A11
Lyn DA. 2008. Turbulence models for sediment transport engineering. In *Sedimentation Engineering*, ed. MH García. American Society of Coastal Engineers

Machicoane N, Volk R. 2016. Lagrangian velocity and acceleration correlations of large inertial particles in a closed turbulent flow. *Phys. Fluids* 28(3):035113
MacLeod M, Arp HPH, Tekman MB, Jahnke A. 2021. The global threat from plastic pollution. *Science* 373(6550):61–65
Marchioli C, Fantoni M, Soldati A. 2007. Influence of added mass on anomalous high rise velocity of light particles in cellular flow field: a note on the paper by Maxey (1987). *Phys. Fluids* 19(9):098101
Masselink G, Puleo JA. 2006. Swash-zone morphodynamics. *Continental Shelf Res.* 26(5):661–80
Mathai V, Lohse D, Sun C. 2020. Bubbly and buoyant particle–laden turbulent flows. *Annu. Rev. Condens. Matter Phys.* 11:529–59
Maxey MR, Riley JJ. 1983. Equation of motion for a small rigid sphere in a nonuniform flow. *Phys. Fluids* 26(4):883–89
Mazzitelli IM, Lohse D. 2004. Lagrangian statistics for fluid particles and bubbles in turbulence. *New J. Phys.* 6:203
McWilliams JC, Sullivan PP, Moeng CH. 1997. Langmuir turbulence in the ocean. *J. Fluid Mech.* 334:1–30
Michels J, Stippkugel A, Lenz M, Wirtz K, Engel A. 2018. Rapid aggregation of biofilm-covered microplastics with marine biogenic particles. *Proc. R. Soc. B* 285(1885):20181203
Moon S, Martin LMA, Kim S, Zhang Q, Zhang R, et al. 2024. Direct observation and identification of nanoplastics in ocean water. *Sci. Adv.* 10(4):eadh1675
Moore CJ, Moore SL, Leecaster MK, Weisberg SB. 2001. A comparison of plastic and plankton in the North Pacific central gyre. *Mar. Pollut. Bull.* 42(12):1297–300
Moulton M, Suanda SH, Garwood JC, Kumar N, Fewings MR, Pringle JM. 2023. Exchange of plankton, pollutants, and particles across the nearshore region. *Annu. Rev. Mar. Sci.* 15:167–202
Napper I, Thompson R. 2023. Plastics and the environment. *Annu. Rev. Environ. Resour.* 48:55–79
Ni R. 2024. Deformation and breakup of bubbles and drops in turbulence. *Annu. Rev. Fluid Mech.* 56:319–47
Nielsen P. 1984. On the motion of suspended sand particles. *J. Geophys. Res.* 89(C1):616–26
Núñez P, Romano A, García-Alba J, Besio G, Medina R. 2023. Wave-induced cross-shore distribution of different densities, shapes, and sizes of plastic debris in coastal environments: a laboratory experiment. *Mar. Pollut. Bull.* 187:114561
Obbard RW, Sadri S, Wong YQ, Khitun AA, Baker I, Thompson RC. 2014. Global warming releases microplastic legacy frozen in Arctic Sea ice. *Earths Future* 2(6):315–20
OECD (Organisation for Economic Co-operation and Development). 2024. *Policy Scenarios for Eliminating Plastic Pollution by 2040.* OECD
Onink V, Jongedijk CE, Hoffman MJ, van Sebille E, Laufkötter C. 2021. Global simulations of marine plastic transport show plastic trapping in coastal zones. *Environ. Res. Lett.* 16(6):064053
Onink V, van Sebille E, Laufkötter C. 2022. Empirical Lagrangian parametrization for wind-driven mixing of buoyant particles at the ocean surface. *Geosci. Model Dev.* 15(5):1995–2012
Ouellette NT, O'Malley PJJ, Gollub JP. 2008. Transport of finite-sized particles in chaotic flow. *Phys. Rev. Lett.* 101(17):174504
Parrella F, Brizzolara S, Holzner M, Mitrano DM. 2024. Impact of heteroaggregation between microplastics and algae on particle vertical transport. *Nat. Water* 2(6):541–52
Peirson WL, Banner ML. 2003. Aqueous surface layer flows induced by microscale breaking wind waves. *J. Fluid Mech.* 479:1–38
Perlin M, Choi W, Tian Z. 2013. Breaking waves in deep and intermediate waters. *Annu. Rev. Fluid Mech.* 45:115–45
Pizzo N, Melville WK, Deike L. 2019. Lagrangian transport by nonbreaking and breaking deep-water waves at the ocean surface. *J. Phys. Oceanogr.* 49(4):983–92
Poorte REG, Biesheuvel A. 2002. Experiments on the motion of gas bubbles in turbulence generated by an active grid. *J. Fluid Mech.* 461:127–54
Porter A, Lyons BP, Galloway TS, Lewis C. 2018. Role of marine snows in microplastic fate and bioavailability. *Environ. Sci. Technol.* 52(12):7111–19
Poulain M, Mercier MJ, Brach L, Martignac M, Routaboul C, et al. 2019. Small microplastics as a main contributor to plastic mass balance in the North Atlantic subtropical gyre. *Environ. Sci. Technol.* 53(3):1157–64

Poulain-Zarcos M, Pujara N, Verhille G, Mercier MJ. 2024. Laboratory experiments related to marine plastic pollution: a review of past work and future directions. *C. R. Phys.* 25(S3):235–66
Protière S. 2023. Particle rafts and armored droplets. *Annu. Rev. Fluid Mech.* 55:459–80
Pujara N, Thiffeault JL. 2023. Wave-averaged motion of small particles in surface gravity waves: effect of particle shape on orientation, drift, and dispersion. *Phys. Rev. Fluids* 8(7):074801
Qiao F, Yuan Y, Yang Y, Zheng Q, Xia C, Ma J. 2004. Wave-induced mixing in the upper ocean: distribution and application to a global ocean circulation model. *Geophys. Res. Lett.* 31(11):L11303
Rahmani M, Gupta A, Jofre L. 2022. Aggregation of microplastic and biogenic particles in upper-ocean turbulence. *Int. J. Multiphase Flow* 157:104253
Rainville EJ, Thomson J, Moulton M, Derakhti M. 2025. Surfing transport of buoyant objects observed in the nearshore. Preprint, ESS Open Archive. **https://doi.org/10.22541/essoar.173878078.86107499/v1**
Rapizo H, Durrant TH, Babanin AV. 2018. An assessment of the impact of surface currents on wave modeling in the Southern Ocean. *Ocean Dyn.* 68(8):939–55
Ruiz-Orejón LF, Sardá R, Ramis-Pujol J. 2018. Now, you see me: high concentrations of floating plastic debris in the coastal waters of the Balearic Islands (Spain). *Mar. Pollut. Bull.* 133:636–46
Rumer RR, Crissman RD, Wake A. 1979. *Ice transport in Great Lakes*. Rep., Great Lakes Environmental Research Laboratory, NOAA
Ruth DJ, Néel B, Erinin MA, Mazzatenta M, Jaquette R, et al. 2022. Three-dimensional measurements of air entrainment and enhanced bubble transport during wave breaking. *Geophys. Res. Lett.* 49(16):e2022GL099436
Ruth DJ, Vernet M, Perrard S, Deike L. 2021. The effect of nonlinear drag on the rise velocity of bubbles in turbulence. *J. Fluid Mech.* 924:A2
Sanness Salmon HR, Baker LJ, Kozarek JL, Coletti F. 2023. Effect of shape and size on the transport of floating particles on the free surface in a natural stream. *Water Resour. Res.* 59(10):e2023WR035716
Santamaria F, Boffetta G, Martins Afonso M, Mazzino A, Onorato M, Pugliese D. 2013. Stokes drift for inertial particles transported by water waves. *Europhys. Lett.* 102(1):14003
Scherer C, Brennholt N, Reifferscheid G, Wagner M. 2017. Feeding type and development drive the ingestion of microplastics by freshwater invertebrates. *Sci. Rep.* 7(1):17006
Schumacher J, Eckhardt B. 2002. Clustering dynamics of Lagrangian tracers in free-surface flows. *Phys. Rev. E* 66(1):017303
Shaw DB, Li Q, Nunes JK, Deike L. 2023. Ocean emission of microplastic. *PNAS Nexus* 2(10):pgad296
Song Y, Rau MJ. 2022. A novel method to study the fragmentation behavior of marine snow aggregates in controlled shear flow. *Limnol. Oceanogr. Methods* 20(10):618–32
Squires KD, Eaton JK. 1991. Measurements of particle dispersion obtained from direct numerical simulations of isotropic turbulence. *J. Fluid Mech.* 226:1–35
Stark M. 2022. Plausibility checks are needed in microplastic research to prevent misinterpretations. *Environ. Sci. Technol.* 56(24):17495–97
Sun Y, Bakker T, Ruf C, Pan Y. 2023. Effects of microplastics and surfactants on surface roughness of water waves. *Sci. Rep.* 13(1):1978
Sunberg LKC, DiBenedetto MH, Ouellette NT, Koseff JR. 2024. Parametric study of the dispersion of inertial ellipsoidal particles in a wave-current flow. *Phys. Rev. Fluids* 9(3):034302
Sutherland BR, Dhaliwal MS, Thai D, Li Y, Gingras M, Konhauser K. 2023a. Suspended clay and surfactants enhance buoyant microplastic settling. *Commun. Earth Environ.* 4(1):393
Sutherland BR, DiBenedetto M, Kaminski A, van den Bremer T. 2023b. Fluid dynamics challenges in predicting plastic pollution transport in the ocean: a perspective. *Phys. Rev. Fluids* 8(7):070701
Sutherland P, Melville WK. 2015. Field measurements of surface and near-surface turbulence in the presence of breaking waves. *J. Phys. Oceanogr.* 45(4):943–65
Taylor GI. 1922. Diffusion by continuous movements. *Proc. Lond. Math. Soc.* s2-20(1):196–212
Taylor JR. 2018. Accumulation and subduction of buoyant material at submesoscale fronts. *J. Phys. Oceanogr.* 48(6):1233–41
Teixeira MAC, Belcher SE. 2002. On the distortion of turbulence by a progressive surface wave. *J. Fluid Mech.* 458:229–67

Thompson RC, Courtene-Jones W, Boucher J, Pahl S, Raubenheimer K, Koelmans AA. 2024. Twenty years of microplastic pollution research—what have we learned? *Science* 386(6720):eadl2746
Thompson RC, Olsen Y, Mitchell RP, Davis A, Rowland SJ, et al. 2004. Lost at sea: Where is all the plastic? *Science* 304(5672):838
Thomson J, Schwendeman MS, Zippel SF, Moghimi S, Gemmrich J, Rogers WE. 2016. Wave-breaking turbulence in the ocean surface layer. *J. Phys. Oceanogr.* 46(6):1857–70
Tinklenberg A, Guala M, Coletti F. 2023. Thin disks falling in air. *J. Fluid Mech.* 962:A3
van den Bremer TS, Breivik Ø. 2018. Stokes drift. *Phil. Trans. R. Soc. A* 376(2111):20170104
van Sebille E, Aliani S, Law KL, Maximenko N, Alsina JM, et al. 2020. The physical oceanography of the transport of floating marine debris. *Environ. Res. Lett.* 15(2):023003
van Sebille E, Wilcox C, Lebreton L, Maximenko N, Hardesty BD, et al. 2015. A global inventory of small floating plastic debris. *Environ. Res. Lett.* 10(12):124006
Verhille G. 2022. Deformability of discs in turbulence. *J. Fluid Mech.* 933:A3
Veron F. 2015. Ocean spray. *Annu. Rev. Fluid Mech.* 47:507–38
Voth GA, Soldati A. 2017. Anisotropic particles in turbulence. *Annu. Rev. Fluid Mech.* 49:249–76
Wang LP, Maxey MR. 1993. Settling velocity and concentration distribution of heavy particles in homogeneous isotropic turbulence. *J. Fluid Mech.* 256:27–68
Wang T, Zhao S, Zhu L, McWilliams JC, Galgani L, et al. 2022. Accumulation, transformation and transport of microplastics in estuarine fronts. *Nat. Rev. Earth Environ.* 3(11):795–805
Watkins L, Sullivan PJ, Walter MT. 2021. What you net depends on if you grab: a meta-analysis of sampling method's impact on measured aquatic microplastic concentration. *Environ. Sci. Technol.* 55(19):12930–42
Weiss L, Ludwig W, Heussner S, Canals M, Ghiglione JF, et al. 2021. The missing ocean plastic sink: gone with the rivers. *Science* 373(6550):107–11
Wieczorek AM, Croot PL, Lombard F, Sheahan JN, Doyle TK. 2019. Microplastic ingestion by gelatinous zooplankton may lower efficiency of the biological pump. *Environ. Sci. Technol.* 53(9):5387–95
Will JB, Mathai V, Huisman SG, Lohse D, Sun C, Krug D. 2021. Kinematics and dynamics of freely rising spheroids at high Reynolds numbers. *J. Fluid Mech.* 912:A16
Woodall LC, Sanchez-Vidal A, Canals M, Paterson GL, Coppock R, et al. 2014. The deep sea is a major sink for microplastic debris. *R. Soc. Open Sci.* 1(4):140317
Worm B, Lotze HK, Jubinville I, Wilcox C, Jambeck J. 2017. Plastic as a persistent marine pollutant. *Annu. Rev. Environ. Resour.* 42:1–26
Xiao Q, Calvert R, Yan SQ, Adcock TAA, van den Bremer TS. 2024. Surface gravity wave-induced drift of floating objects in the diffraction regime. *J. Fluid Mech.* 980:A27
Xiao Q, McAllister ML, Adcock TAA, van den Bremer TS. 2025. Laboratory study of the enhanced wave-induced drift of large rectangular floating objects. *J. Fluid Mech.* 1008:A18
Zippel SF, Maksym T, Scully M, Sutherland P, Dumont D. 2020. Measurements of enhanced near-surface turbulence under windrows. *J. Phys. Oceanogr.* 50(1):197–215